LAWRENCE
LIVERMORE
NATIONAL
LABORATORY

LLNL-JRNL-676434

Broadband Processing in a Noisy Shallow Ocean Environment: A Particle Filtering Approach

J. V. Candy

August 20, 2015

IEEE Journal on Oceanic Engineering

Disclaimer

Broadband Processing in a Noisy Shallow Ocean Environment: A Particle Filtering Approach

J. V. Candy, *Fellow, IEEE*

Abstract

When a broadband source propagates sound in a shallow ocean the received data can become quite complicated due to temperature related sound speed variations and therefore a highly dispersive environment. Noise and uncertainties disrupt this already chaotic environment even further because disturbances propagate through the same inherent acoustic channel. The broadband (signal) estimation/detection problem can be decomposed into a set of narrowband solutions that are processed separately and then combined to achieve more enhancement of signal levels than that available from a single frequency thereby allowing more information to be extracted leading to a more reliable source detection. A Bayesian solution to the broadband modal function tracking, pressure-field enhancement and source detection problem is developed that leads to nonparametric estimates of desired posterior distributions enabling the estimation of useful statistics and an improved processor/detector. To investigate the processor capabilities, we synthesize an ensemble of noisy, broadband, shallow ocean measurements to evaluate its overall performance using an information theoretical metric for the pre-processor and the receiver operating characteristic curve for the detector.

KEYWORDS: littoral region, normal-modes, broadband Bayesian processor, sequential Monte Carlo, particle filter, performance metrics, information theory, Kullback-Leibler divergence, sequential detection

I. INTRODUCTION

Sound propagation in the shallow ocean initiated by sources significantly complicate the analysis of received acoustic data especially when they are broadband. Temperature changes resulting sound speed variations can cause highly dispersive propagation resulting in a statistically nonstationary signal. Highly correlated propagation channels obscure the problem of extracting target signals from disturbances and noise even further. Noise and inherent uncertainties whether ambient, distant shipping, wind blown surface generated disrupt this uncertain environment primarily because propagation is through the same acoustic channel. Broadband data can provide a wealth of information about the medium, target, disturbances and noise that is not necessarily available from narrowband data commonly acquired in shallow regions making it highly desirable—if this information can be extracted.

The characterization of broadband sources has long been a problem with keen interest in the ocean acoustic community. Initially, the work of many began with a simple temporal matched-filter approach [1], [2]-[3] where a

This work performed under the auspices of the U.S. Department of Energy by the Lawrence Livermore National Laboratory under Contract DE-AC52-07NA27344.

The author is with the Lawrence Livermore National Laboratory, Livermore, CA 94551, (email: candy1@llnl.gov)

known source location was used to provide a replica employed to match to the measured data. An alternative to the temporal matched-filter approach evolved as a natural extension to model-based, matched-field/matched mode processing encompassing the matching of a predicted to a measured pressure-field under an assumed source location [4]-[7]. Matched-mode processing of broadband source signals also offers improved signal levels capable of not only localizing the target, but also estimating its broadband temporal spectrum [8]-[13].

Employing a vertical hydrophone sensor array, the improved *SNR* of broadband acoustic pressure-field measurements using a multichannel Bayesian technique to estimate or filter the noisy measurement data is discussed. Here the approach is developed for the broadband source using a normal-mode propagation model. Propagation theory predicts that a different modal structure evolves for each spectral line; therefore, it is not surprising that the multichannel solution to this problem results in a scheme that requires a bank of processors—each employing its own underlying modal structure for the narrow frequency band that it operates. Following [14], the Bayesian solution of using state-space forward propagators is briefly discussed. It is shown that each state-space processor is naturally decoupled in modal space and recombined in the measurement space without any approximations (decoupled gains of [14]) to provide improved signal level estimates. That is, the estimated or equivalently "filtered" modal/pressure-field data with improved *SNR* evolves providing a solution to the signal/measurement *enhancement problem* and subsequent broadband *source detection problem*.

It has already been shown that the state-space representation can be utilized for signal level enhancement to propagate modal and range functions in both the narrowband and broadband cases [13], [14]. In the random case, a stochastic model evolves allowing the inclusion of uncertain phenomena such as noise and modeling errors in a consistent manner. In our case, the measurement noise can be lumped into an additive noise term to represent the near-field acoustic noise field, flow noise on the hydrophones and electronic noise, whereas the modal/range uncertainty can be lumped as a process noise term to represent sound speed profile errors, correlated noise from distant shipping, errors in the boundary conditions, sea state effects and ocean inhomogeneities [15]-[17].

In this paper we develop a Bayesian solution to the signal enhancement/detection problem or equivalently improved (higher signal-to-noise (*SNR*)) estimation of both modal functions and pressure-field measurements of noisy, uncertain, broadband acoustic signals in a shallow ocean environment using a Markov chain Monte Carlo (*MCMC*) sampling approach [18]. These techniques lead to a nonparametric representation of the posterior modal (state/measurement) distributions and their associated statistics that are then used to develop a sequential source detection technique. This contribution is sixfold, we: (1) develop a sequential, model-based, Bayesian solution to the broadband signal enhancement problem in a shallow ocean using a normal-mode propagation model; (2) illustrate the underlying multi-modal nature of the posterior probability mass functions (*PMF*) for simulated data leading to an improved pre-processor; (3) evaluate the pre-processor performance by applying an information theoretic metric along with the usual classical "sanity" tests; (4) perform ensemble (100-members) testing to bound the sequential Bayesian estimates and analyze their underlying statistics; (5) develop a sequential solution to the broadband source detection problem; and (6) evaluate detection performance by developing the associated receiver operating characteristic (*ROC*) curve.

This approach leads directly to the so-called *particle filter* (*PF*) that is a sequential *MCMC* Bayesian processor capable of providing reasonable performance for a multi-modal problem estimating a nonparametric representation of the posterior distribution [18]-[20]. It can be thought of simply as producing a histogram-like estimate of the underlying distribution (probability mass) that can be exploited to extract the desired signals through statistical inference (e.g. conditional mean). This processor has a set of unique capabilities when compared to other processors that rely on an assumption of a unimodal distribution (e.g. Kalman filter). The particle filter: (1) is capable of providing a solution to the signal enhancement problem when the underlying distributions are multi-modal; (2) is able to incorporate the addition of any noise sources and uncertainties that are statistically viable; (3) incorporates statistical sampling techniques in which the entities or clouds of "particles" are developed based on the underlying ocean propagation (modes/pressure-field) representations; (4) can extract improved modal/pressure-field estimates with reasonable error statistics for this problem; (5) leads to the estimation of important statistics such as the maximum a-posteriori or minimum mean-squared error estimates of the states (modes), measurements (pressure-field) and inherent parameters (not currently included); and (6) when used as a pre-processor becomes an integral part of the solution to wide variety of applications (e.g. detection, classification, localization, and source tracking [21], [22]). Here we apply it directly to the broadband source detection problem illustrating its applicability to enhance the required signals that results in improved detection performance.

We provide a brief discussion of the broadband problem and the underlying state-space model structures in Sec. II. Next in Sec. III, we develop the broadband Bayesian processor showing that it can provide a Bayesian solution to the signal level (modes/pressure-field) enhancement problem as well as the broadband source detection problem. Data synthesized from an ensemble of shallow ocean simulations create a set of noisy, broadband, pressure-field data in Sec. IV. These data are used to illustrate the applicability of the pre-processor/detector as well as evaluate its overall performance. We summarize our results in the final section.

II. BROADBAND STATE-SPACE PROPAGATORS

In this section we briefly summarize the development of a broadband (state-space) propagator. This propagator is embedded in the Bayesian particle filter solution. Next we briefly discuss the broadband normal-mode extension and then the transformation of this underlying model to state-space form.

A. Broadband Normal-Modes

It is well-known [2], [9], [15] in ocean acoustics that the pressure-field solution to the Helmholtz equation under the appropriate assumptions can be expressed as the sum of normal modes. The resulting narrowband modal solution has been extended to include a broadband source, $s(t)$, with corresponding spectrum, $S_s(\omega)$ by [9]-[12]. In this case, the ocean medium is specified by its *Green's* function (impulse response) which can be expressed in terms of the inherent normal modes spanning the water column

$$\mathcal{G}(r,z,\omega) := \sum_m \mathcal{H}_o\left(\kappa_r(m)r\right)\phi_m(z_s,\omega)\phi_m(z,\omega) \tag{1}$$

where $\mathcal{H}_o$ is the zeroth order Hankel function; $\kappa_r(m)$ is the horizontal wavenumber associated with the m-th mode; ω is the set of broadband temporal source frequencies, r and z_s are the source range/depth coordinates, respectively and $\phi_m(z,\omega)$ is the m-th modal or eigensolution, satisfying the *vertical* or *depth* equation obtained through separation of variables applied to the Helmholtz equation [2] given by

$$\frac{d^2}{dz^2}\phi_m(z,\omega) + \kappa_z^2(m,\omega)\phi_m(z,\omega) = 0. \tag{2}$$

The wavenumbers satisfy the corresponding *dispersion relation*

$$\frac{\omega^2}{c^2(z)} = \kappa_r^2(m,\omega) + \kappa_z^2(m,\omega), \qquad m = 1,\ldots,M \tag{3}$$

where κ_z is the depth-dependent vertical wavenumber and $c(z)$ the depth-dependent sound speed profile.

The continuous source spectrum can be decomposed into a set of narrowband components assuming an impulse sampled spectrum at each spectral bin, $q\triangle\omega$. Therefore, extracting just the q-th source frequency, we have that $S_s(\omega_q)$ can be interpreted as a single narrowband impulse at ω_q with amplitude, $a_q = \triangle\omega|S(\omega_q)|$. The normal-mode solution to the Helmholtz equation for the broadband source problem can be decomposed into a series of narrowband solutions $\{\omega_q\}; q = 1,\cdots,Q$, such that the resulting pressure-field is

$$p(r,z,\omega_q) = \sum_{m=1}^{M_q} a_q \mathcal{H}_o\left(\kappa_r(m,q)r\right)\phi_m(z_s,\omega_q)\phi_m(z,\omega_q) \tag{4}$$

where M_q is the number of modes spanning the water column at frequency ω_q with the corresponding dispersion relation satisfying

$$\kappa_r^2(m,q) = \frac{\omega_q^2}{c^2(z)} - \kappa_z^2(m,q) \text{ for } m = 1,\ldots,M_q \tag{5}$$

and the pressure-field at depth z and time t can be expressed in terms of the bilateral inverse (discrete) Fourier transform as

$$p(r,z,t) = \int_{-\infty}^{\infty} p(r,z,\omega)e^{j\omega t}d\omega \approx \frac{1}{Q}\sum_{q=-(Q-1)}^{Q-1} p(r,z,\omega_q)e^{j\omega_q t} \tag{6}$$

B. State-Space Propagators

It is well-known [13], [14] that the state-space propagators for the narrowband pressure-field can be obtained from the depth relationship and the broadband extensions discussed. Following the development in [14], we define the modal state vector for the m-th mode, at frequency ω_q, as

$$\mathbf{\Phi}_m(z,\omega_q) = \begin{bmatrix} \phi_m(z,\omega_q) \\ ----- \\ \frac{d}{dz}\phi_m(z,\omega_q) \end{bmatrix}, \quad m = 1,\cdots,M_q. \tag{7}$$

The depth-only relation of Eq. 2 can now be written in state-space form as

$$\frac{d}{dz}\mathbf{\Phi}_m(z,\omega_q) = \mathbf{A}_m(z,\omega_q)\mathbf{\Phi}_m(z,\omega_q), \tag{8}$$

where

$$\mathbf{A}_m(z,\omega_q) = \begin{bmatrix} 0 & 1 \\ -\kappa_z^2(m,q) & 0 \end{bmatrix}, \quad m = 1,\cdots,M_q. \tag{9}$$

Expanding over the M_q modes at each narrowband frequency ω_q component, we have that

$$\frac{d}{dz}\mathbf{\Phi}(z,\omega_q) = \mathbf{A}(z,\omega_q)\mathbf{\Phi}(z,\omega_q) = \begin{bmatrix} \mathbf{A}_1(z,\omega_q) & \cdots & O \\ \vdots & \ddots & \vdots \\ O & \cdots & \mathbf{A}_{M_q}(z,\omega_q) \end{bmatrix} \mathbf{\Phi}(z,\omega_q) \tag{10}$$

with the single frequency state vector defined by

$$\mathbf{\Phi}^T(z,\omega_q) := \left[\mathbf{\Phi}_1^T(z,\omega_q)\cdots\mathbf{\Phi}_{M_q}^T(z,\omega_q)\right] \tag{11}$$

for $\mathbf{\Phi}(z,\omega_q) \in \mathcal{R}^{2M_q\times 1}$.

Suppose we further assume an L-element vertical sensor array, then $z \to z_\ell$, $\ell = 1,\cdots,L$ and therefore, the pressure-field at the array for the q-th temporal frequency of Eq. 4 becomes

$$p(r_s,z_\ell,\omega_q) = \mathbf{C}_{q+1}^T(r_s,z_s,\omega_q)\mathbf{\Phi}(z_\ell,\omega_q) \tag{12}$$

with the *measurement matrix* for the "known" source range (from array) and depth, (r_s,z_s), we obtain

$$\mathbf{C}_{q+1}^T(r_s,z_s,\omega_q) = \left[\beta_1(r_s,z_s,\omega_q) \;\; 0 | \cdots | \beta_{M_q}(r_s,z_s,\omega_q) \;\; 0\right] \tag{13}$$

where $\mathbf{C}_q^T \in \mathcal{C}^{1\times 2M_q}$ and

$$\beta_m(r_s,z_s,\omega_q) := a_q\mathcal{H}_o\big(\kappa_r(m,q)r_s\big)\phi_m(z_s,\omega_q) \tag{14}$$

Equations 8 and 12 constitute the *state equation* and *measurement equation* at temporal frequency ω_q. This model is *only* valid for a single temporal frequency, ω_q. Extending it to the broadband case, we see from Eq. 4 and 5 that as the temporal frequency (ω_q) changes, the corresponding number of modes (M_q) and horizontal wavenumbers ($\kappa_r(m,q)$) at each frequency also change. Thus, the state-space propagator for the broadband case must allow for this frequency and wavenumber dependence.

With this issue in mind, we now define the overall *broadband state-space propagator* as

$$\frac{d}{dz}\mathbf{\Phi}(z,\Omega) = \mathbf{A}(z,\Omega)\mathbf{\Phi}(z,\Omega) \tag{15}$$

with $\mathbf{A}(z,\Omega) = diag\left[\mathbf{A}(z,\omega_0)\cdots\mathbf{A}(z,\omega_{Q-1})\right]$, $\mathbf{A}(z,\omega) \in \mathbf{R}^{2M\times 2M}$, and

$$\mathbf{\Phi}(z_\ell, \Omega) := [\mathbf{\Phi}(z_\ell, \omega_0) \ \cdots \ \mathbf{\Phi}(z_\ell, \omega_{Q-1})]^T \tag{16}$$

for $\mathbf{\Phi}(z_\ell, \Omega) \in \mathbf{R}^{2M \times 1}$ and $\mathbf{A}_m(z, \omega_q)$ as in Eq. 9 with $q = 0, \ldots, Q-1; \ m = 1, \ldots, M_q$. The parameter M, the total number of single frequency modes, is given by $M = \sum_{q=1}^{Q} M_q$. Note that we use the parameter "Ω" to signify the entire set of discrete temporal frequencies, $\Omega := \{\omega_q\}, q = 0, \cdots, Q-1$.

Thus, the overall broadband pressure measurement relation at time t is given by (see Appendix B for details)

$$p(z_\ell, \Omega) := p(r_s, z_\ell) = \mathbf{C}(r_s, z_s, \Omega)\mathbf{\Phi}(z_\ell, \Omega) \tag{17}$$

with

$$\mathbf{C}(r_s, z_s, \Omega) = \left[\frac{1}{Q}\mathbf{C}_1^T(r_s, z_s, \omega_0)e^{j\omega_0 t} \ \cdots \ \frac{1}{Q}\mathbf{C}_Q^T(r_s, z_s, \omega_{Q-1})e^{j\omega_{Q-1} t}\right] \tag{18}$$

for $\mathbf{C} \in \mathcal{C}^{1 \times 2M}$.

This completes the summary of the *deterministic*, broadband, state-space forward propagator, next we consider adding uncertainties to this representation.

C. Stochastic State-Space Propagators

The stochastic nature of this broadband ocean acoustic problem requires the introduction of *uncertainties* not just in the overall propagation of noise and disturbances, but also uncertainties in the underlying modal model parameters. For these reasons we incorporate additive stochastic processes to capture the noisy, varying shallow ocean medium, that is, discretizing Eq. 15 using central differences for numerical stability [21] (see Appendix) gives

$$\begin{aligned} \mathbf{\Phi}(z_\ell, \Omega) &= \mathbf{A}(z_{\ell-1}, \Omega)\mathbf{\Phi}(z_{\ell-1}, \Omega) + \mathbf{w}(z_{\ell-1}, \Omega) \\ p(z_\ell, \Omega) &= \mathbf{C}(r_s, z_s, \Omega)\mathbf{\Phi}(z_\ell, \Omega) + v(z_\ell, \Omega) \end{aligned} \tag{19}$$

where $\mathbf{w}$ is an independent, uncorrelated, zero-mean process with spectral covariance $\mathbf{R}_{ww}(z_\ell, \Omega)$, $v \sim \mathcal{N}(0, R_{vv}(z_\ell, \Omega))$ and *initial* modal state vector distributed Gaussian with specified mean and spectral covariance as: $\mathbf{\Phi}(z_0, \Omega) \sim \mathcal{N}(\overline{\mathbf{\Phi}}(z_0, \Omega), \mathbf{R}_{\phi\phi}(z_0, \Omega))$.

The process noise/uncertainty source $\mathbf{w}$ is a random input to the broadband (state-space) ocean acoustic model capturing the random nature of the variety of stochastic processes and disturbances discussed previously that propagate through the uncertain medium in the same acoustic channel as the signal source. It enables a pragmatic synthesis of the propagation uncertainties [17]. The measurement noise v at each sensor is modeled by a zero-mean, uncorrelated (white) sequence representing instrumentation uncertainties. This completes the fundamental stochastic state-space representation providing the required ocean acoustic models for the subsequent processor.

III. BROADBAND BAYESIAN PROCESSOR

For our pressure-field/modal function estimation problem, we define the underlying broadband pressure-field/modal function *signal enhancement problem* as:

GIVEN a set of noisy broadband pressure-field measurements, $P_\ell := \{p(z_1,\Omega),\cdots,p(z_\ell,\Omega)\}$ and the underlying stochastic model of Eq. 19, FIND an estimate of the posterior distribution, $\hat{\Pr}[\mathbf{\Phi}(z_\ell,\Omega)|P_\ell]$ and infer the corresponding enhanced estimates of the broadband modal functions, $\hat{\mathbf{\Phi}}(z_\ell,\Omega)$ and pressure-field, $\hat{p}(z_\ell,\Omega)$.

The solution to this problem can be obtained by estimating the joint *a posteriori* distribution applying Bayes' theorem, that is, the joint probability of the broadband modal functions at the ℓ-th depth based on the set of pressure-field measurements up to z_ℓ is given by

$$\Pr\big[\mathbf{\Phi}_\ell|P_\ell\big] = \frac{\Pr\big[P_\ell|\mathbf{\Phi}_\ell\big] \times \Pr\big[\mathbf{\Phi}_\ell\big]}{\Pr\big[P_\ell\big]} \tag{20}$$

where $\mathbf{\Phi}_\ell := \{\mathbf{\Phi}(z_1,\Omega)\cdots,\mathbf{\Phi}(z_\ell,\Omega)\}$ is the set of broadband modal functions (states) and P_ℓ is the set of broadband measurements up to and including $p(z_\ell,\Omega)$.

Following [18], the measurement *likelihood* distribution, that is, the joint set of measurements up to and including the ℓ-th based on the set of broadband modal functions at depth z_ℓ can be factored using Bayes' rule as

$$\Pr\big[P_\ell|\mathbf{\Phi}_\ell\big] = \Pr\big[p(z_\ell,\Omega)|\mathbf{\Phi}(z_\ell,\Omega)\big] \times \Pr\big[P_{\ell-1}|\mathbf{\Phi}_{\ell-1}\big] \tag{21}$$

under the assumed independence of $p(z_\ell,\Omega)$ with $P_{\ell-1}$ and $\mathbf{\Phi}_{\ell-1}$ and $\mathbf{\Phi}(z_\ell,\Omega)$ with $P_{\ell-1}$.

Similarly, the joint *prior* modal distribution at depth z_ℓ can also be factored to give the (modal) *transition* distribution

$$\Pr\big[\mathbf{\Phi}_\ell\big] = \Pr\big[\mathbf{\Phi}(z_\ell,\Omega),\mathbf{\Phi}_{\ell-1}\big] = \Pr\big[\mathbf{\Phi}(z_\ell,\Omega)|\mathbf{\Phi}(z_{\ell-1},\Omega)\big] \times \Pr\big[\mathbf{\Phi}_{\ell-1}\big] \tag{22}$$

under the first order Markov assumption, while that for the joint *evidence* is factored as

$$\Pr\big[\mathbf{P}_\ell\big] = \Pr\big[p(z_\ell,\Omega),\mathbf{P}_{\ell-1}\big] = \Pr\big[p(z_\ell,\Omega)|\mathbf{P}(z_{\ell-1},\Omega)\big] \times \Pr\big[\mathbf{P}_{\ell-1}\big] \tag{23}$$

Substituting these relations into Eq. 20, cancelling like-terms, assuming conditional independence and recognizing the Bayes' relation for the previous step, $\Pr\big[\mathbf{\Phi}_{\ell-1}|P_{\ell-1}\big]$, we obtain the sequential Bayes' expression for the joint posterior density of the set of broadband modal functions based on the pressure-field measurements as

$$\Pr\big[\mathbf{\Phi}_\ell|P_\ell\big] = \Big(\frac{\Pr\big[p(z_\ell,\Omega)|\mathbf{\Phi}(z_\ell,\Omega)\big] \times \Pr\big[\mathbf{\Phi}(z_\ell,\Omega)|\mathbf{\Phi}(z_{\ell-1},\Omega)\big]}{\Pr\big[p(z_\ell,\Omega)|P_{\ell-1}\big]}\Big) \times \Pr\big[\mathbf{\Phi}_{\ell-1}|P_{\ell-1}\big] \tag{24}$$

consisting of the *measurement* likelihood, *modal* transition prior and evidence (for details see [18]).

A. Broadband Particle Filters

One approach to estimate the required posterior distribution of Eq. 24 from noisy broadband measurements is to develop the so-called particle filter (*PF*) [18]. A *particle filter* is a completely different approach to nonlinear filtering that is capable of characterizing multi-modal distributions. In fact, it might be easier to think of the *PF* as a histogram or kernel density-like estimator [18] in the sense that it is an estimated empirical probability mass function (*PMF*) that approximates the desired posterior distribution such that inferences can be performed and statistics extracted directly. Here the idea is a change in thinking where we attempt to develop an empirical estimation of the posterior distribution following a purely Bayesian approach using Monte Carlo (*MC*) sampling theory as its enabling foundation [18]. As one might expect, the computational burden of the *PF* is much higher than that of other processors, since it must provide an estimate of the underlying state posterior distribution state-by-state at each z_ℓ-step along with the fact that the number of samples to characterize the distribution is equal to the number of particles (N_p). The estimated *empirical posterior distribution* for the broadband signal enhancement problem is given by

$$\hat{\Pr}[\mathbf{\Phi}(z_\ell,\Omega)|P_\ell] = \sum_{i=1}^{N_p} \mathcal{W}_i(z_\ell,\Omega) \times \delta\big(\mathbf{\Phi}(z_\ell,\Omega) - \mathbf{\Phi}_i(z_\ell,\Omega)\big) \tag{25}$$

where the weights and posterior distribution estimated by the *PF* are given by

P_ℓ is the set of batch pressure-field measurements,

$\mathcal{W}_i(z_\ell,\Omega)$ is the *i*-th broadband weight (normalized) at depth z_ℓ

$\mathbf{\Phi}_i(z_\ell,\Omega)$ is the *i*-th particle of the broadband modal function at depth z_ℓ

Once the underlying posterior is available, then estimates of important statistics can be extracted directly. For instance, the maximum a posteriori (*MAP*) estimate is found by locating a particular particle $\mathbf{\Phi}_i(z_\ell,\Omega)$ corresponding to the maximum of the *PMF*at that depth, that is,

$$\hat{\mathbf{\Phi}}_{MAP}(z_\ell,\Omega) = \max_i \ \hat{\Pr}\Big[\mathbf{\Phi}_i(z_\ell,\Omega)|P_\ell\Big] \tag{26}$$

while the conditional mean (*CM*) or equivalently the minimum mean-squared error (*MMSE*) estimate is estimated by

$$\hat{\mathbf{\Phi}}_{CM}(z_\ell,\Omega) \approx \frac{1}{N_p}\sum_{i=1}^{N_p} \mathcal{W}_i(z_\ell,\Omega) \times \mathbf{\Phi}_i(z_\ell,\Omega) \tag{27}$$

The Bayesian solution for this problem is based on determining the associated broadband weighting function that leads to the estimated empirical posterior distribution. A sampling or equivalently importance distribution

$\mathrm{I}\Big(\mathbf{\Phi}(z_\ell,\Omega)|P_\ell\Big)$ is *selected* first, then the weight (unnormalized) is determined by the ratio of the desired posterior to this choice, [18]

$$W\Big(z_\ell,\Omega\Big) := \frac{\Pr\Big[\mathbf{\Phi}(z_\ell,\Omega)|P_\ell\Big]}{\mathrm{I}\Big(\mathbf{\Phi}(z_\ell,\Omega)|P_\ell\Big)}$$

which can be expanded using Bayes' rule of Eq. 20 to provide the "sequential" generic weight

$$W\Big(z_\ell,\Omega\Big) := W\Big(z_{\ell-1},\Omega\Big) \times \frac{\Pr\Big[p(z_\ell,\Omega)|\mathbf{\Phi}(z_\ell,\Omega)\Big] \times \Pr\Big[\mathbf{\Phi}(z_\ell,\Omega)|\mathbf{\Phi}(z_{\ell-1},\Omega)\Big]}{\mathrm{I}\Big(\mathbf{\Phi}(z_\ell,\Omega)|P_\ell\Big)} \tag{28}$$

where the numerator is the product of the *likelihood* and the state *transition* probability.

B. Bayesian Performance Metrics

Particle filters are basically developed to provide estimates of the underlying posterior distributions for the problem under investigation in order to extract meaningful statistics. Compared to the usual model-based (Kalman) processors which utilize their inherent "optimality" property (zero-mean, uncorrelated residuals) to assess performance, the estimated posterior of the *PF* must somehow be compared to the true distribution of the underlying process it is to estimate. One way to achieve this comparison, is to utilize the associated *divergence statistic* of the well-known Kullback-Leibler information as a metric [23]. Much effort has been devoted to this comparison problem with the most significant results evolving from the information theoretic approach to distribution assessment [23], [24].

For our problem suppose $\Pr[\mathbf{\Phi}(z_\ell,\Omega)|P_\ell]$ is the *true* posterior *PMF* and $\hat{\Pr}[\mathbf{\Phi}_i(z_\ell,\Omega)|P_\ell]$ is the estimated (particle) distribution, then the *Kullback-Leibler* (*KL*) information quantity of the true distribution relative to the estimated is defined by

$$\begin{aligned}\mathcal{I}_{KL}\left(\Pr[\mathbf{\Phi}(z_\ell,\Omega)|P_\ell];\hat{\Pr}[\mathbf{\Phi}_i(z_\ell,\Omega)|P_\ell]\right) &:= E_{\mathbf{\Phi}}\left\{\ln\frac{\Pr[\mathbf{\Phi}(z_\ell,\Omega)|P_\ell]}{\hat{\Pr}[\mathbf{\Phi}_i(z_\ell,\Omega)|P_\ell]}\right\} \\ &= \sum_{i=1}^{N_p}\ln\frac{\Pr[\mathbf{\Phi}(z_\ell,\Omega)|P_\ell]}{\hat{\Pr}[\mathbf{\Phi}_i(z_\ell,\Omega)|P_\ell]} \times \Pr[\mathbf{\Phi}(z_\ell,\Omega)|P_\ell]\end{aligned} \tag{29}$$

The *KL* possesses some very useful properties. It satisfies, perhaps its most important property from a distribution comparison viewpoint—when the true distribution and its estimate are *close* (or identical), then the information quantity is

$$\mathcal{I}_{KL}\left(\Pr[\mathbf{\Phi}(z_\ell,\Omega)|P_\ell];\hat{\Pr}[\mathbf{\Phi}_i(z_\ell,\Omega)|P_\ell]\right) = 0 \Leftrightarrow \Pr[\mathbf{\Phi}(z_\ell,\Omega)|P_\ell] = \hat{\Pr}[\mathbf{\Phi}_i(z_\ell,\Omega)|P_\ell] \quad \forall i \tag{30}$$

This property infers that as the *estimated* posterior distribution approaches the *true* distribution, then the value of the *KL* approaches *zero* (minimum).

Our interest lies in comparing two probability distributions to determine "how close" they are to one another. Even though, the $\mathcal{I}_{KL}$ does quantify the *difference* between the true and estimated distribution, it is not a distance metric to answer this question due to its lack of symmetry. However, the *Kullback divergence* (*KD*) defined by

$$\begin{aligned}\mathcal{J}_{KD}\Big(\text{Pr}[\mathbf{\Phi}(z_\ell,\Omega)|P_\ell];\hat{\text{Pr}}[\mathbf{\Phi}_i(z_\ell,\Omega)|P_\ell]\Big) &:= \mathcal{I}_{KL}\Big(\text{Pr}[\mathbf{\Phi}(z_\ell,\Omega)|P_\ell];\hat{\text{Pr}}[\mathbf{\Phi}_i(z_\ell,\Omega)|P_\ell]\Big)\\ &+ \mathcal{I}_{KL}\Big(\hat{\text{Pr}}[\mathbf{\Phi}_i(z_\ell,\Omega)|P_\ell];\text{Pr}[\mathbf{\Phi}(z_\ell,\Omega)|P_\ell]\Big)\end{aligned} \tag{31}$$

is a *distance metric* between distributions indicating "how close" one distribution is to the other or from our perspective, "how well does it approximate" the posterior. Thus, the *KD* is a very important metric that can be applied to assess the performance of Bayesian processors providing a measure between the true and estimated posterior distributions that we apply to our broadband problem.

C. Bootstrap Particle Filters

There are a variety of *PF* algorithms available based on the choice of the importance distribution [18]-[20]. Perhaps the simplest is the *bootstrap* technique [25]. The *PF* design for our problem using the bootstrap approach employs the state transition probability as its importance distribution, that is,

$$\text{I}\Big(\mathbf{\Phi}(z_\ell,\Omega)|P_\ell\Big) := \text{Pr}\Big[\mathbf{\Phi}(z_\ell,\Omega)|\mathbf{\Phi}(z_{\ell-1},\Omega)\Big] \tag{32}$$

Substituting this expression into Eq. 28 leads to the weighting function

$$W\Big(z_\ell,\Omega\Big) = W\Big(z_{\ell-1},\Omega\Big)\times\text{Pr}\Big[p(z_\ell,\Omega)|\mathbf{\Phi}(z_\ell,\Omega)\Big] \tag{33}$$

which is simply the *likelihood distribution*.

For the bootstrap implementation, we draw samples from the state *transition* distribution using the dynamic modal model of Eq. 19 driven by the process uncertainty $\mathbf{w}_i(z_{\ell-1},\Omega)$ to generate the set of particles, $\{\mathbf{\Phi}_i(z_\ell,\Omega)\}$ for each $i=1,\cdots,N_p$.

The *likelihood*, on the other hand, is determined from the pressure-field measurement model for each mode giving the likelihood (assuming Gaussian measurement noise) as

$$\text{Pr}[p(z_\ell,\Omega)|\mathbf{\Phi}_i(z_\ell,\Omega)] = \frac{1}{\sqrt{2\pi R_{vv}(\Omega)}}\times\exp\Big\{-\frac{1}{2R_{vv}(\Omega)}\Big(p(z_\ell,\Omega)-\mathbf{C}(r_s,z_s,\Omega)\mathbf{\Phi}_i(z_\ell,\Omega)\Big)^2\Big\} \tag{34}$$

Thus, we can estimate the posterior distribution using a sequential Monte Carlo approach and construct a *bootstrap particle filter* [18] using the following steps:

- Initialize: $\mathbf{\Phi}_i(z_0,\Omega),\mathbf{w}_i(z_0,\Omega)\sim\mathcal{N}\big(0,\mathbf{R}_{ww}(z_0,\Omega)\big),v(z_0,\Omega)\sim\mathcal{N}\big(0,\mathbf{R}_{vv}(z_0,\Omega)\big),W_i(z_0,\Omega)=1/N_p;i=1,\cdots,N_p$

- State Transition: $\mathbf{\Phi}_i(z_\ell,\Omega) = \mathbf{A}(z_{\ell-1},\Omega)\mathbf{\Phi}_i(z_{\ell-1},\Omega) + \mathbf{w}_i(z_{\ell-1},\Omega)$

- Likelihood Probability: $\Pr[p(z_\ell,\Omega)|\mathbf{\Phi}_i(z_\ell,\Omega)]$ of Eq. 34

- Weights: $W_i(z_\ell,\Omega) = W_i(z_{\ell-1},\Omega) \times \Pr[p(z_\ell,\Omega)|\mathbf{\Phi}_i(z_\ell,\Omega)]$

- Normalize: $\mathcal{W}_i(z_\ell,\Omega) = \frac{W_i(z_\ell,\Omega)}{\sum_{i=1}^{N_p} W_i(z_\ell,\Omega)}$

- Resample: $\begin{cases} \hat{\mathbf{\Phi}}_i(z_\ell,\Omega) \Rightarrow \mathbf{\Phi}_i(z_\ell,\Omega) & N_{eff} \le N_\tau \quad \text{(resample)} \\ & N_{eff} > N_\tau \quad \text{(no resample)} \end{cases}$

- Posterior: $\hat{\Pr}[\mathbf{\Phi}_i(z_\ell,\Omega)|P_\ell] = \sum_{i=1}^{N_p} \mathcal{W}_i(z_\ell,\Omega)\delta(\mathbf{\Phi}(z_\ell,\Omega) - \hat{\mathbf{\Phi}}_i(z_\ell,\Omega))$

- *MAP* Estimate: $\hat{\mathbf{\Phi}}_{MAP}(z,\Omega) = \max_i \hat{\Pr}[\mathbf{\Phi}_i(z_\ell,\Omega)|P_\ell]$

- *CM* Estimate: $\hat{\mathbf{\Phi}}_{CM}(z,\Omega) = \frac{1}{N_p}\sum_{i=1}^{N_p} \mathcal{W}_i(z_\ell,\Omega) \times \mathbf{\Phi}_i(z_\ell,\Omega)$

A detailed flow diagram of this particle filter (bootstrap) algorithm is shown in Fig. 1 illustrating the prediction and update steps along with a resampling algorithm to provide convergence (more details can be found in [18]-[20]). We see from this figure that after initialization the broadband modal model is used to generate the particles during the *prediction* step. These particles, $\mathbf{\Phi}_i(z_\ell,\Omega)$, are then incorporated into the likelihood distribution providing the *update* step.

Resampling of the particles is usually required to prevent degeneracy of the associated weights which increase in variance at each depth making it impossible to avoid the degradation. *Resampling* consists of processing the particles with their associated weights duplicating those of large weights (probabilities) and discarding those of small weights. In this way only those particles of highest probabilities (importance) are retained enabling a coalescence at the peaks of the resulting posterior distribution while mitigating the degradation. A measure based on the coefficient of variation, the *effective* particle sample size given by

$$N_{eff} = \frac{1}{\sum_{i=1}^{N_p} W_i^2(z_\ell,\Omega)} \tag{35}$$

is the underlying *decision statistic* such that when its value is less than a pre-determined threshold resampling is

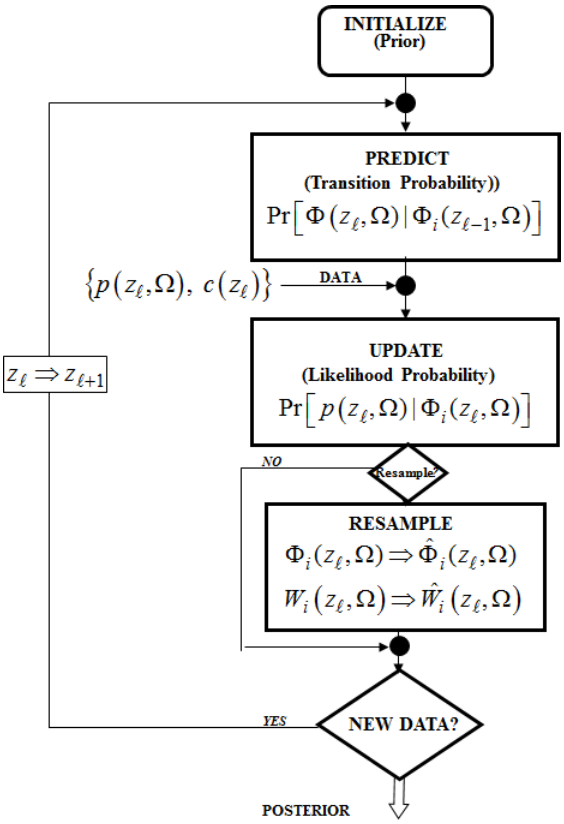

Fig. 1. Broadband Bayesian sequential (bootstrap) particle filter algorithm: Initialization, prediction (modal forward propagator) state transition probability, update (data) likelihood probability, resample decision function (resampling), estimated posterior probability output.

performed (see [20] for more details).

We should also note from the structure of the *PF* algorithm that each mode (two-states) is driven by the modal process noise/uncertainty vector $\mathbf{w}_i(z_\ell)$. This process coupled with the underlying block diagonal structure of $\mathbf{A}(z_\ell,\Omega)$ enables a *parallel* construct of the overall processor that is eventually combined by the measurement model of the likelihood distribution. Here, in contrast to the approximate (unimodal) model-based (Kalman) scheme of [14], *no* approximations are required to obtain this overall block-diagonal structure and parallel implementation.

D. Sequential Detection

In this section, we develop a sequential detector that incorporates the particle filter to solve the basic problem of detecting a broadband source from noisy pressure-field measurements. For our decision problem, we define the underlying broadband *source detection problem* as:

GIVEN a set of noisy broadband pressure-field measurements, $P_\ell := \{p(z_1,\Omega),\cdots,p(z_\ell,\Omega)\}$ with the underlying stochastic model of Eq. 19 and the "data likelihood" distribution, $\Pr[p(z_\ell,\Omega)|P_{\ell-1}]$, DECIDE whether or not the broadband source is present.

This is a binary decision problem; therefore, we are to test the hypothesis of whether the noisy pressure-field measurements have evolved from a broadband source or not. The corresponding binary hypothesis test is

$$\begin{aligned}\mathcal{H}_0:\ p(z_\ell,\Omega) &= v(z_\ell,\Omega) && \text{[NOISE]}\\ \mathcal{H}_1:\ p(z_\ell,\Omega) &= \mathbf{C}(r_s,z_s,\Omega)\mathbf{\Phi}_i(z_\ell,\Omega)+v(z_\ell,\Omega) && \text{[SOURCE]}\end{aligned} \tag{36}$$

An optimal solution to this decision problem is based on applying the *Neyman-Pearson theorem* leading to the likelihood-ratio [26], [27] defined by

$$\mathcal{L}(P_L) := \frac{\text{Pr}[P_L|\mathcal{H}_1]}{\text{Pr}[P_L|\mathcal{H}_0]} \begin{array}{c}\mathcal{H}_1\\ >\\ <\\ \mathcal{H}_0\end{array} \mathcal{T} \tag{37}$$

where $P_L = \{p(z_1,\Omega),\cdots,p(z_L,\Omega)\}$ with threshold $\mathcal{T}$.

Expanding the likelihood-ratio for each depth, we obtain

$$\mathcal{L}(P_L) = \frac{\text{Pr}[p(z_1,\Omega),\cdots,p(z_L,\Omega)|\mathcal{H}_1]}{\text{Pr}[p(z_1,\Omega),\cdots,p(z_L,\Omega)|\mathcal{H}_0]} \tag{38}$$

From the chain rule of probability and Bayes' theorem [28], we have that

$$\text{Pr}[P_L|\mathcal{H}_i] = \text{Pr}[p(z_L,\Omega),P_{L-1}|\mathcal{H}_i] = \text{Pr}[p(z_L,\Omega)|P_{L-1},\mathcal{H}_i]\times\text{Pr}[P_{L-1}|\mathcal{H}_i] \tag{39}$$

Substituting these expressions into the likelihood-ratio above, replacing $L\rightarrow\ell$ and grouping we obtain the sequential form of likelihood-ratio as [27]

$$\mathcal{L}(P_\ell) = \left(\frac{\text{Pr}[p(z_{\ell-1},\Omega)|\mathcal{H}_1]}{\text{Pr}[p(z_{\ell-1},\Omega)|\mathcal{H}_0]}\right)\times\frac{\text{Pr}[p(z_\ell,\Omega)|p(z_{\ell-1},\Omega),\mathcal{H}_1]}{\text{Pr}[p(z_\ell,\Omega)|p(z_{\ell-1},\Omega),\mathcal{H}_0]} \tag{40}$$

or

$$\mathcal{L}\big(p(z_\ell,\Omega)\big) = \mathcal{L}\big(p(z_{\ell-1},\Omega)\big)\times\frac{\text{Pr}[p(z_\ell,\Omega)|p(z_{\ell-1},\Omega),\mathcal{H}_1]}{\text{Pr}[p(z_\ell,\Omega)|p(z_{\ell-1},\Omega),\mathcal{H}_0]} \tag{41}$$

Taking logarithms simplifies the computations; therefore, we define $\Lambda\big(p(z_\ell,\Omega)\big) := \ln\mathcal{L}\big(p(z_\ell,\Omega)\big)$ to obtain the *sequential log-likelihood-ratio* decision function for the broadband source detection problem as

$$\begin{aligned}\Lambda\big(p(z_\ell,\Omega)\big) &= \Lambda\big(p(z_{\ell-1},\Omega)\big)+\ln\text{Pr}[p(z_\ell,\Omega)|p(z_{\ell-1},\Omega),\mathcal{H}_1]\\ &- \ln\text{Pr}[p(z_\ell,\Omega)|p(z_{\ell-1},\Omega),\mathcal{H}_0]\end{aligned} \tag{42}$$

To complete this development we require thresholds that lead to the Wald *sequential probability-ratio test* [27] for

$$\begin{aligned}\Lambda\big(p(z_\ell,\Omega)\big) &> \ln\mathcal{T}_1(\ell) && \text{Accept}\quad\mathcal{H}_1\\ \ln\mathcal{T}_0(\ell)\ \leq\Lambda\big(p(z_\ell,\Omega)\big) &\leq \ln\mathcal{T}_1(\ell) && \text{Continue}\\ \Lambda\big(p(z_\ell,\Omega)\big) &< \ln\mathcal{T}_0(\ell) && \text{Accept}\quad\mathcal{H}_0\end{aligned}$$

These thresholds can be obtained from an operating point (P_{FA},P_{DET}) on the associated *ROC* curve obtained through simulation or experimental data and are specified by

$$\mathcal{T}_0(\ell) = \frac{1 - \mathrm{P}_{\mathrm{DET}}(\ell)}{\mathrm{P}_{\mathrm{FA}}(\ell)} \qquad \mathcal{T}_1(\ell) = \frac{\mathrm{P}_{DET}(\ell)}{\mathrm{P}_{\mathrm{FA}}(\ell)} \tag{43}$$

For our problem, the particle filter is used to estimate the desired *data likelihood* distribution based on the nonparametric estimate of the posterior distribution, that is, we require an estimate of the

$$\hat{\Pr}[p(z_\ell, \Omega)|p(z_{\ell-1}, \Omega); \mathcal{H}_\ell]; \ \ell = 0, 1 \tag{44}$$

under each hypothesis of Eq. 36.

It has been shown from the well-known Chapman-Kolomogorov relation [28] that

$$\Pr[p(z_\ell, \Omega)|p(z_{\ell-1}, \Omega)] = \int \Pr\big[p(z_\ell, \Omega)|\mathbf{\Phi}(z_\ell, \Omega)\big] \times \Pr[\mathbf{\Phi}(z_\ell, \Omega)|P_{\ell-1}] \ d\Phi(z_\ell, \Omega) \tag{45}$$

coupled with the assumption of a "perfect sampler" for the one-step prediction distribution

$$\hat{\Pr}\big[\mathbf{\Phi}(z_\ell, \Omega)|P_{\ell-1}\big] = \frac{1}{N_p} \sum_{i=1}^{N_p} \delta\Big(\mathbf{\Phi}(z_\ell, \Omega) - \mathbf{\Phi}_i(z_\ell, \Omega)\Big)$$

gives the *estimated* data likelihood as

$$\begin{aligned} &\hat{\Pr}[p(z_\ell, \Omega)|p(z_{\ell-1}, \Omega)] \approx \\ &\frac{1}{N_p} \sum_{i=1}^{N_p} \int \Pr[p(z_\ell, \Omega)|\mathbf{\Phi}(z_\ell, \Omega)] \times \delta\big(\mathbf{\Phi}(z_\ell, \Omega) - \mathbf{\Phi}_i(z_\ell, \Omega)\big) \ d\Phi(z_\ell, \Omega) = \frac{1}{N_p} \sum_{i=1}^{N_p} \Pr[p(z_\ell, \Omega)|\mathbf{\Phi}_i(z_\ell, \Omega)] \end{aligned} \tag{46}$$

If we further assume a first-order Markov process $\big(P_{\ell-1} \rightarrow p(z_{\ell-1}, \Omega)\big)$ and choose the importance distribution to be the state transition $\mathrm{I}(\mathbf{\Phi}(z_\ell, \Omega)|\mathbf{\Phi}(z_{\ell-1}, \Omega), P_{\ell-1}) \rightarrow \Pr\big[\mathbf{\Phi}(z_\ell, \Omega)|\mathbf{\Phi}(z_{\ell-1}, \Omega)\big]$, then the bootstrap *PF* results with weight, $\mathcal{W}_i(z_\ell, \Omega) \rightarrow \Pr\big[p(z_\ell, \Omega)|\mathbf{\Phi}_i(z_\ell, \Omega)\big]$. Therefore, the data likelihood can be approximated by

$$\hat{\Pr}\big[p(z_\ell, \Omega)|p(z_{\ell-1}, \Omega)\big] = \frac{1}{N_p} \sum_{i=1}^{N_p} \Pr\big[p(z_\ell, \Omega)|\mathbf{\Phi}_i(z_\ell, \Omega)\big] \approx \frac{1}{N_p} \sum_{i=1}^{N_p} \mathcal{W}_i(z_\ell, \Omega) =: \overline{\mathcal{W}}(z_\ell, \Omega) \tag{47}$$

where $\overline{\mathcal{W}}$ is the ensemble mean of the weight at each depth [29], [30].

Thus, the corresponding *sequential log-likelihood decision function* for the broadband source detection problem is

$$\Lambda\big(p(z_\ell, \Omega)\big) = \Lambda\big(p(z_{\ell-1}, \Omega)\big) + \ln \overline{\mathcal{W}}(z_\ell, \Omega; \mathcal{H}_1) - \ln \overline{\mathcal{W}}(z_\ell, \Omega; \mathcal{H}_0) \tag{48}$$

This completes the development of the sequential detector that is applied to our simulated data.

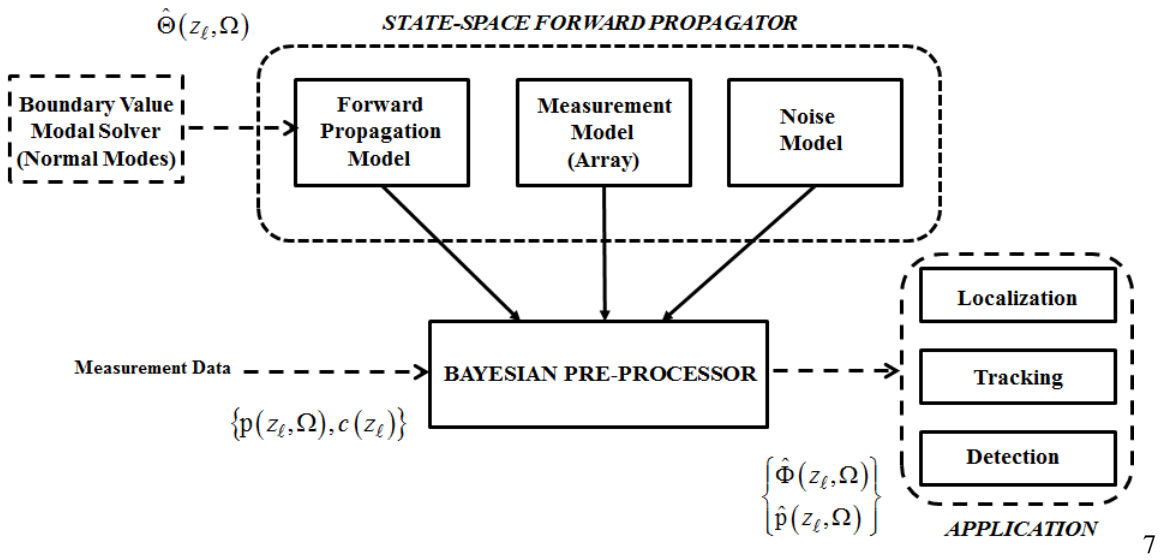

Fig. 2. Bayesian processor design: Boundary value solver provides initial state-space parameters for modal forward propagation, measurement and noise/uncertainty models (state-space forward propagator) and data provides the inputs of pressure-field and sound-speed. Bayesian pre-processor outputs can be incorporated into potential ocean acoustic applications such as localization, tracking and detection.

IV. BROADBAND BAYESIAN DESIGN FOR A SHALLOW OCEAN

In this section we discuss the application of the Bayesian processor to ensemble data synthesized by a broadband normal-mode model using the state-space forward propagator and the underlying stochastic representation of the previous section. In order to develop the propagator we *first* must define the shallow water boundary value problem and solve it to obtain the parameters required for the processor.

It is important to realize that the state-space "forward" propagators do *not* offer an alternative solution to the Helmholtz equation, but rather use the parameters *from* the boundary value solution to obtain a set of initial conditions/parameters for propagator construction and signal processing. Therefore, in order to implement the processor model parameters (e.g. wavenumbers, modal coefficients, temporal frequencies, sound-speed and other scale factors) of the ocean medium under investigation must be provided or else jointly estimated in a parametrically adaptive scheme [21]. This is not uncommon in any of the model-based approaches [16] and is illustrated in Fig. 2. Model parameters are obtained using, for example, SNAP [31], KRAKEN [32], SAFARI [33] providing initial parameter estimates and inputs to the Bayesian processor for a variety of applications.

The problem we consider is that of [14] where a broadband normal-mode model is specified by the SNAP simulation and summarized in [14]. This model is driven by random noise to synthesize noisy broadband pressure-field measurements for *PF* processing. Similar to the model-based (Kalman) processor of [14], the *PF* embeds the broadband normal-mode model and pressure-field models into its structure for statistical sampling generating the clouds of particles. Here we expect the *PF* to track the modal functions and enhance the measurements. We also investigate the classical (zero-mean/whiteness tests) and *MSE* metrics in the analysis to assess the performance of

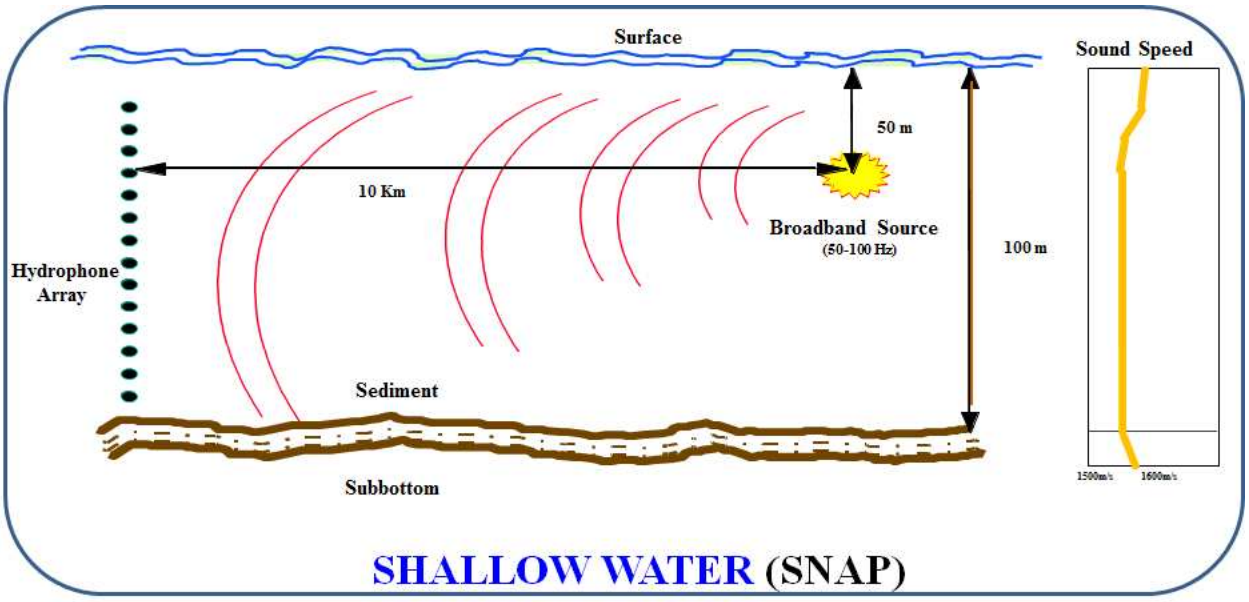

Fig. 3. Broadband shallow water environment problem: Channel ($100m$) with broadband source ($50-100Hz$) located at range $r_s = 10Km$ and depth $z_s = 50m$.

the *PF* as well as the *KD* distance metric discussed in Sec. IIIB.

Let us re-consider the basic shallow water channel of [14] depicted in Figure 3. We assume a flat bottom, range independent three layer environment with a channel depth of $100m$, a sediment depth of $2.5m$ and a subbottom. A vertical line array of 100-sensors with spacing of $\triangle z = 1m$ spans the entire water column and a broadband source of unit amplitude and $50Hz$ bandwidth ranging from $50-100Hz$ in $10Hz$ increments is located at a depth of $50m$ and a range of $10Km$ from the array. The sound speed profile in the water column and the sediment are sketched in the figure and specified along with the other problem parameters (see [14] for details). SNAP, a normal-mode propagation simulator [31] is applied to solve this shallow water problem and executed over the set of discrete temporal source frequencies. This boundary value problem was solved using SNAP and the results at each narrowband frequency are shown in [14].

Next we design the state-space propagator. The parameters obtained from SNAP are now used to construct the broadband state-space and measurement models of Eq. 19. Here we use the set of horizontal wavenumbers, $\{\kappa(m,q)\}, m = 1, \cdots, M_q; q = 1, \cdots, Q$, and sound speed, $\{c(z_\ell)\}$, to implement the state-space models along with the corresponding modal function values, $\{\mathbf{\Phi}(z_s, \omega_q)\}$, as well as the Hankel functions, $\{\mathcal{H}_o(\kappa(m,q)r_s)\}$ to construct the measurement models (modal coefficients).

The final set of parameters for our simulation are the modal and measurement noise covariance matrices required by the stochastic model. The measurement noise is estimated from measured time series data covariance bounds ($\pm 2\sigma$) about its mean, while the process noise is guessed and adjusted during the tuning phase of the processor design. A set of classical metrics to accomplish tuning is discussed next. Once the covariances are specified and

the modal function statistics are estimated from the boundary value problem (*BVP*) outputs, the input (modal) and output (measurement) signal-to-noise ratios (*SNR*) can be calculated from:

$$SNR_{in} := \frac{\text{Cov}\Big(\mathbf{\Phi}_m(z_\ell, \omega_q)\Big)_{m,m}}{\mathbf{R}_{ww}(m,m)}, \quad m = 1, \cdots, M_q$$
$$SNR_{out} := \frac{\mathbf{C}(r_s, z_s, \Omega) \times \text{Cov}\Big(\mathbf{\Phi}(z, \Omega)\Big) \times \mathbf{C}^T(r_s, z_s, \Omega)}{R_{vv}(z, \Omega)} \tag{49}$$

and can be used to specify the simulation.

With this information in hand, a 100-member ensemble of stochastic simulations was performed at $SNR_{in} = 10$ dB (modes) and $SNR_{out} = 0$ dB (pressure-field) based on the SNAP parameters of [14]. We chose to *oversample* the water column to provide detailed spatial resolution permitting a more precise investigation in order to bound processor performance eliminating non-relevant issues for this study. The Bayesian processor is designed using the identical set of parameters used in the shallow water simulation. We can consider this simulation as a performance bound on the best that can be achieved, since the model parameters are precisely known.

1) Classical Performance Metrics: Initially, we develop the processor for a single realization and perform some of the classical statistical tests to ensure the validity of the embedded model. A pragmatic statistical test (in general) for the processor is that the residual sequence should be zero-mean and uncorrelated. In statistical signal processing, this is a standard statistical test to determine whether or not a processor is operating properly, that is, it is used to test whether the residual sequence (difference between the measurement and the processor "predicted" measurement) has a small mean-squared error (*MSE*). Specifically for sequential algorithms, the one-step prediction error (or residual) has the property that the prediction error or equivalently the residual sequence should be zero-mean and uncorrelated (or white). Pragmatically, residuals that satisfy these properties ensure that the embedded model-based processor has "removed" all correlation (of the model) from the data. The remaining measurement (residual) is uncorrelated or equivalently provides no further information about the signal (or model). These properties ensure two conditions: (1) the underlying model is correct; and (2) no further signal information remains to be extracted. In fact, it can be shown that these conditions are a result of the orthogonality condition of the data and its prediction [16]. Indeed this is the case for our 125-*particle design*, since the zero-mean test shows the residual mean to be smaller than the calculated bound ($8.9 \times 10^{-6} < 0.245$) and uncorrelated (white) with only 1.6% of the correlation samples lying outside of the boundaries where more than 5% lying outside is considered non-white or correlated failing the test.

When data are nonstationary, then the *weighted sum-squared residual* (*WSSR*) is a more reliable statistic to use to determine the "whiteness" of the residual error (innovation) sequence [16]. It is a chi-squared statistic that tests the hypothesis of whether or not the residual sequence is statistically uncorrelated or not. The *WSSR* uses this sequence to test whiteness by requiring that the constructed decision function lies below a threshold. If the *WSSR* statistic does lie beneath the calculated threshold, then theoretically, the estimator is considered tuned and the

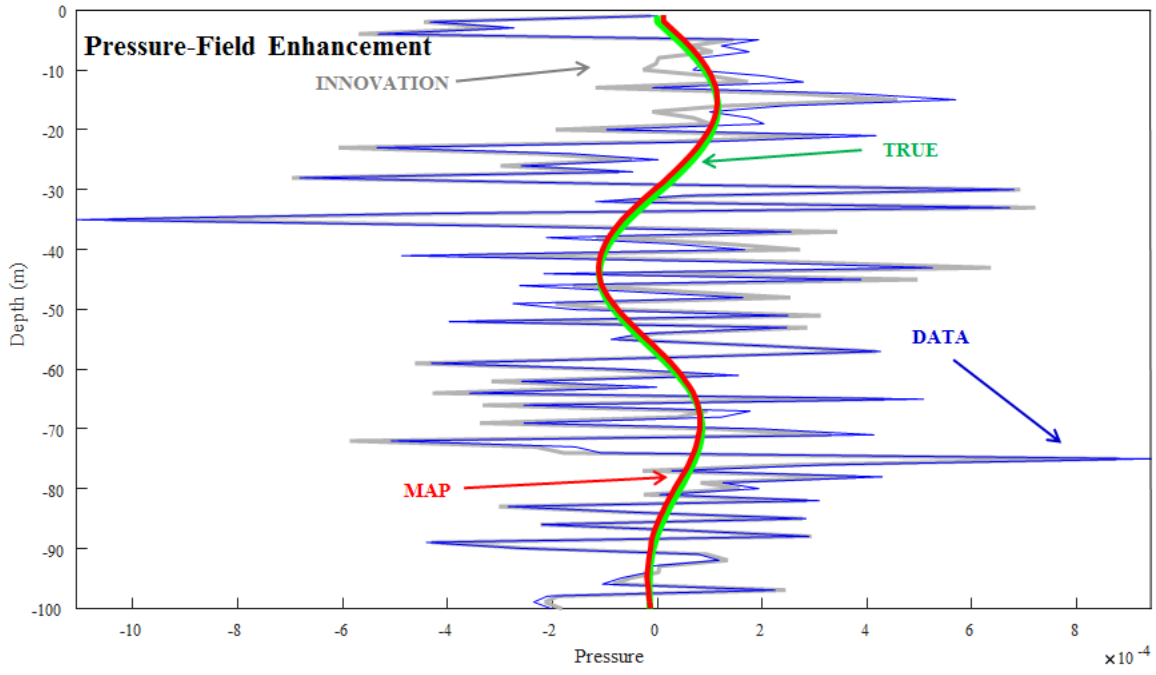

Fig. 4. Broadband shallow water environment pressure-field enhancement: Raw data (*SNR*=0dB), particle filter (125-particles) estimates (MAP, CM) and residual errors (innovations).

embedded model deemed appropriate. More of the *WSSR* details are available in [16], [18]. For our problem, the *WSSR* statistic confirms the whiteness with its decision function lying below the threshold of 81.5 with a 60-sample sliding window.

2) Ensemble Statistics: In order to evaluate the processor performance, we construct a sequence of 100-member realizations and calculate the ensemble statistics. The following results are based on ensemble average estimates, that is, all of the subsequent estimator results have been averaged over the 100-realizations to provide a more meaningful representation of "what could be expected" from the processor when implemented.

The results of the Bayesian design are shown in Fig. 4 where we see the enhanced pressure-field (*MAP*) and the true measurement (mean) as well as the raw data and corresponding residual or innovations sequence as a function of depth. Note from Eq. 19 that the modal estimates $\hat{\mathbf{\Phi}}(z_\ell, \omega_q)$ along with the measurement model, $C^T(r_s, z_s, \omega_q)$ are used to construct the enhanced pressure-field, $\hat{p}(z_\ell, \omega_q)$ at each temporal frequency. To complete the performance analysis, we observe the posterior pressure-field distribution predicted by the *PF* at each depth in Fig. 5. Clearly this distribution is not unimodal, but both *MAP*/*CM* inferences "track" the mean (true) pressure-field quite well. We have also estimated the *KD* statistic which is shown in Figs. 11(a) and 12(a) which will be discussed subsequently.

The estimated modal functions (ensemble averaged) extracted from the noisy pressure-field measurements are shown in Figs. 6 and 7—bounding the estimates we could hope to achieve for this type of data. We use the *annotation*: (Frequency/Mode No.), that is, $M50-1$ is the first modal function at 50Hz frequency. Here we observe

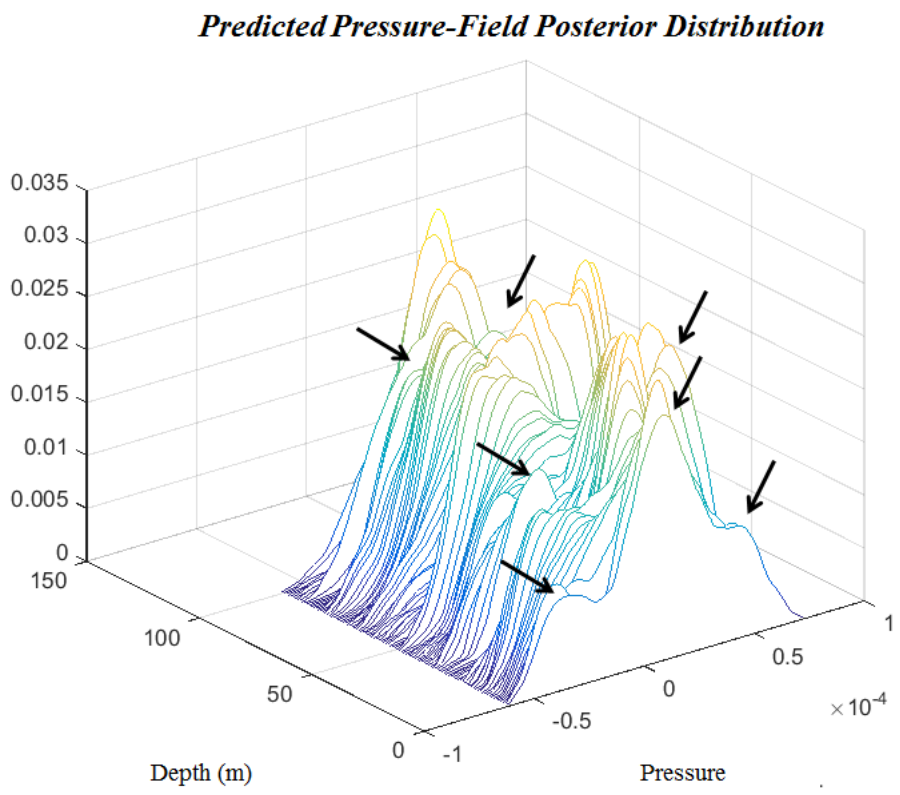

Fig. 5. Predicted pressure-field multi-modal posterior distribution (125-particles) surface (depth vs. pressure vs. probability) indicating a multi-modal surface.

that the *MAP* and *CM* estimates inferred from the predicted posterior modal distributions essentially overlay one another and "track" the true (noise-free) functions very well in spite of the uncertainties in the synthesized modal data. In Fig. 6 we observe the enhanced modal function estimates (ensemble averaged) and uncertain data (DATA) corresponding to the two modes at 50Hz, three at 60Hz and 70Hz and four at 80Hz. In Fig. 7, we see the ensemble estimates for both 90Hz (4 modes) and 100Hz (5 modes). The *RMS MSE* estimates for each of the modal functions are shown in Table I where we observe small modal function tracking errors.

Thus, we see that modal function tracking of the broadband data presents another aspect of the *PF* estimates. We show the posterior *PMF* surfaces (depth vs. modal amplitude vs. probability) for a single realization of modes: Mode: $M50-1$, Mode: $M80-3$ and Mode: $M100-5$ in Figs. 8, 9, 10, respectively. Each surface indicates a multi-modal posterior *PMF* at various depth slices for this nonstationary process. This completes the modal analysis over the ensemble, next we investigate the information theoretical results.

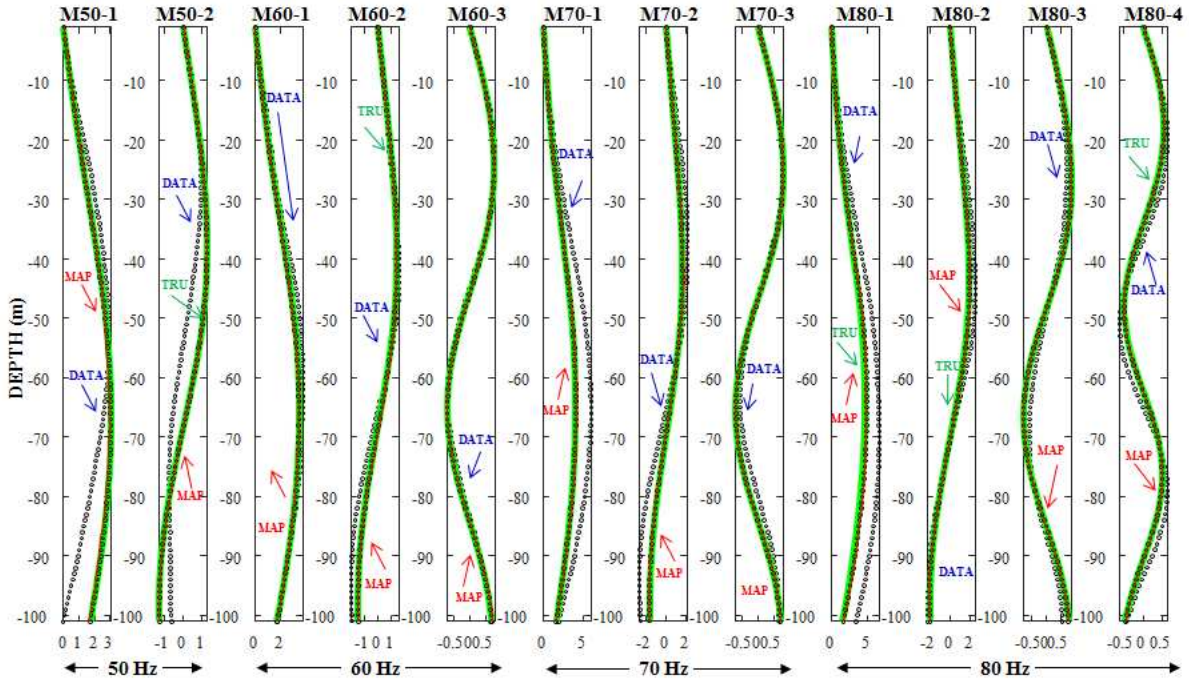

Fig. 6. Broadband shallow water environment mode tracking: Particle filter (125-particles) modal function estimation (MAP, CM) with true (TRUE) and uncertain modes (DATA) at 50-80Hz frequencies.

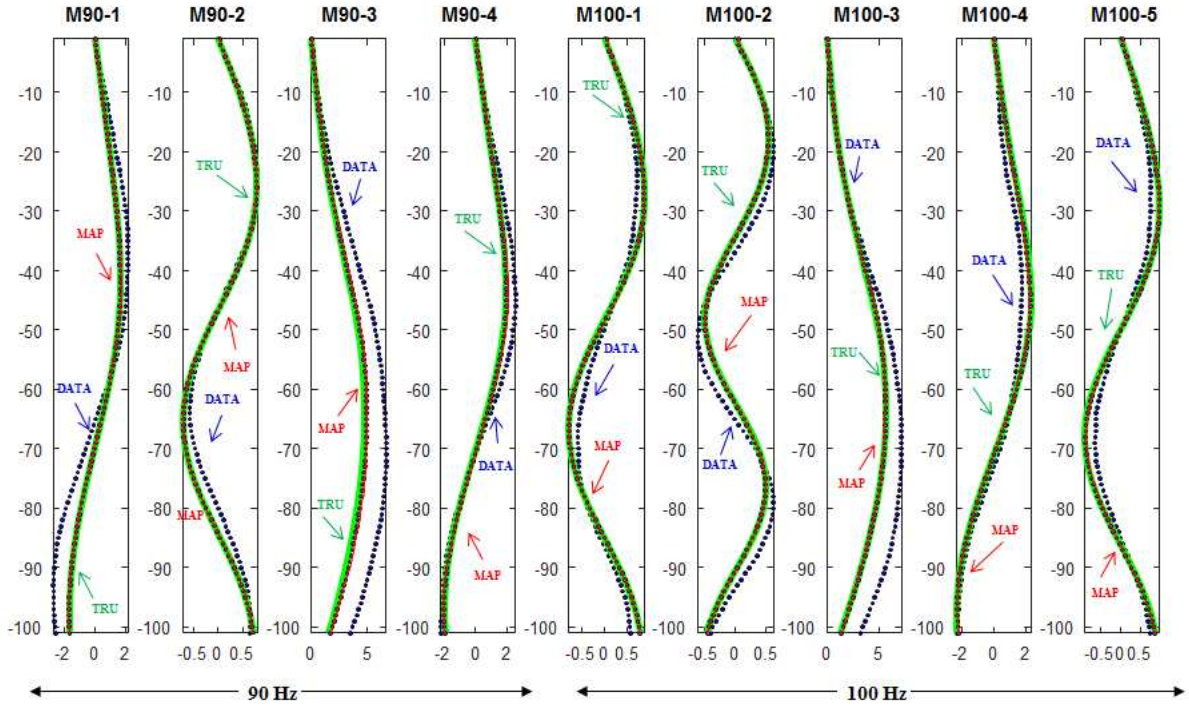

Fig. 7. Broadband shallow water environment mode tracking: Particle filter (125-particles) modal function (21) estimation (MAP, CM) with true (TRUE) and uncertain modes (DATA) at 90-100Hz frequencies.

Table I. Modal Parameters and Tracking Estimation

Particle Filter Performance					
Frequency(Hz)	Mode No.	Modal Coeff.	Wave No.	*MSE*	KLD
50	1	0.122	0.207386	0.03244469	0.02333190
	2	-0.070	0.202489	0.06390081	0.00042730
60	1	0.125	0.249339	0.02057981	0.01498970
	2	-0.063	0.245106	0.02262004	0.00480695
	3	-0.097	0.237639	0.00725442	0.00045842
70	1	0.127	0.291255	0.1173259	0.01173030
	2	-0.057	0.287522	0.07374703	0.00414254
	3	-0.108	0.280907	0.01009431	0.00070735
80	1	0.129	0.333144	0.1376377	0.01020890
	2	-0.052	0.329802	0.03716592	0.00605280
	3	-0.113	0.323913	0.01584901	0.00058421
	4	0.087	0.315526	0.01425319	0.00067141
90	1	0.130	0.375015	0.1104416	0.00699367
	2	-0.047	0.371985	0.02928122	0.00476581
	3	-0.117	0.366685	0.01980555	0.00059496
	4	0.084	0.358997	0.00782307	0.00031112
100	1	0.131	0.416871	0.3176212	0.00648074
	2	-0.043	0.414098	0.06316895	0.00449904
	3	-0.119	0.409278	0.01011795	0.00079068
	4	0.079	0.402279	0.01544138	0.00031464
	5	0.081	0.393399	0.00450539	0.00019501

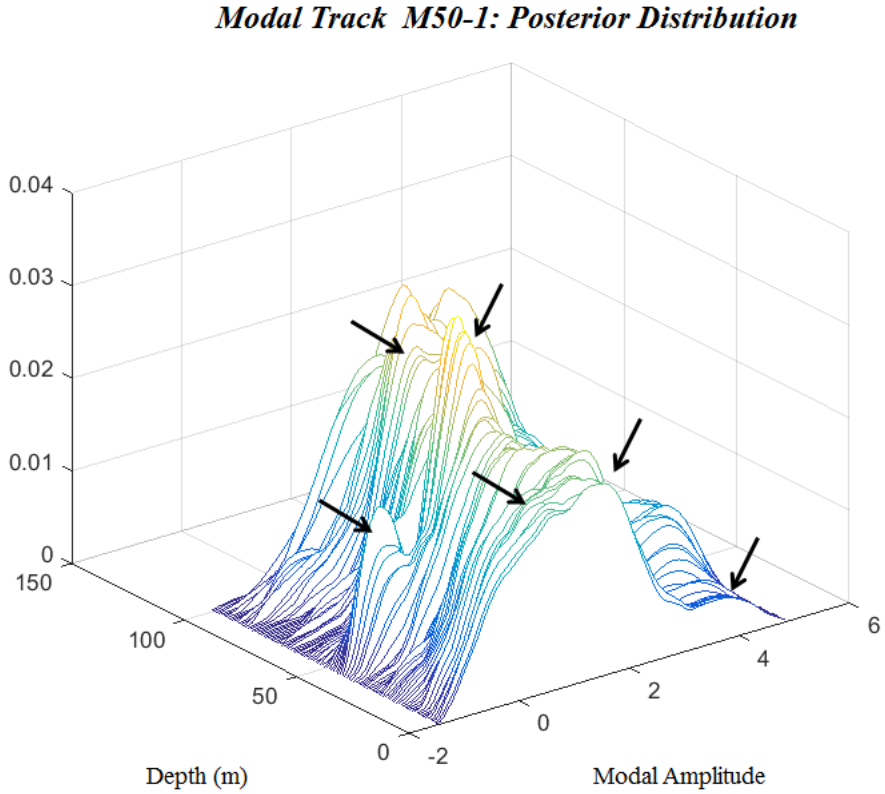

Fig. 8. Estimated multi-modal (arrows) posterior modal distribution (125-particles) surface (depth vs. amplitude vs. probability) for Mode: $M50-1$.

3) Performance Metrics: In this subsection, we investigate the performance of the broadband *PF* over the 100-member ensemble of synthetic pressure-field measurements using the information metrics discussed in Sec. IIIB. The *KD* divergence of Eq. 31 provides us with a metric to determine "how close" the estimated posterior is to the true distribution. Since we have the "true" normal-mode representation (parameters, etc.) available from the simulators (e.g. SNAP, KRAKEN), we can generate realizations from the stochastic forward state-space propagator of Eq. 19. Next, using nonparametric (histogram/kernel density) estimators applied to these realizations empirical *PMF*s are generated to approximate the true distributions for each mode as well as the pressure-field. The empirical *PMF* distributions provided by the *PF* over a set of ensemble runs can then be compared with the true *PMF*s using the *KD* divergence criterion with equality or approximate equality specified by its values *close-to-zero*. As an illustration, we choose time slices of the pressure-field and modal functions (Nos. 1, 11, 21) and estimate these *PMF*s for each as shown in Fig. 11 along with the corresponding *KL* metrics. We used a kernel density estimator (smoothed histogram) from each of the random sequence realizations for the raw synthesized pressure-field data, the true, and *MAP* and *CM* estimates [18].

For the pressure-field shown in Fig. $11a$, it is clear that the broadband enhanced estimates are quite good compared

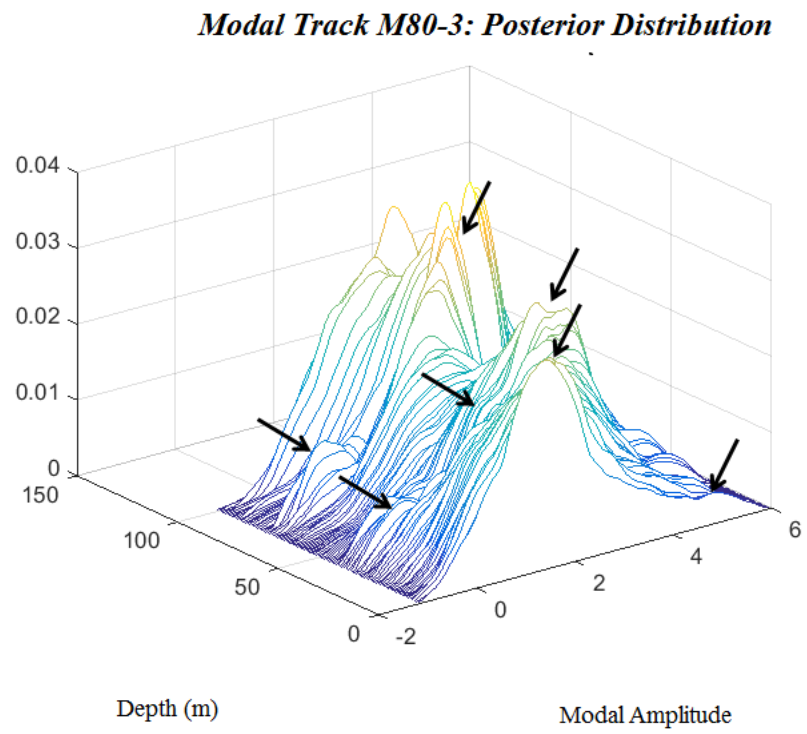

Fig. 9. Estimated multi-modal (arrows) posterior modal distribution (125-particles) surface (depth vs. amplitude vs. probability) for Mode: $M80-3$.

to the noisy data as evidenced by estimated *PMF*s and respective the *KL* divergences of 0.25 (DATA), 0.002 (*MAP*) and 0.0003 (*CM*).

Since the modal process is nonstationary is space (depth z), the multi-modal posterior varies at each discrete depth; therefore, we would have to perform the above analysis on all 21 (42-state) modal functions and the pressure-field at each depth. We can employ the *KL* divergence metric, calculate it at each depth (*PMF*) providing a set of "*KD* trajectories" for the measurement and each mode summarizing the Bayesian processor overall performance. Note that the *perfect PMF* would yield a "zero" (trajectory) at every depth slice. Thus, these trajectories estimate the *KD* for each *PMF* depth slice compressing the information into a single number with summary statistics (mean/median) to follow. The results of the *KD* divergence metric are shown in Fig. 12 comparing each of the multi-modal *PMF*s to the true. We include the median estimates as a single metric performance indicator as well as the corresponding *MSE* estimates in Table I for each mode.

Next we apply the enhanced modal/pressure-field estimator as a pre-processor to solve the broadband source detection problem using the sequential detection approach of Sec. IIID. First, we generate data sets under each hypothesis and then estimate the log-likelihood decision functions for each. From these functions we estimated the corresponding *PMF*s using a kernel density estimator [18] as shown in Fig. 13a. From these distributions we estimated the corresponding *ROC* curve of Fig. 13b and obtained the optimal operating point [26] which was

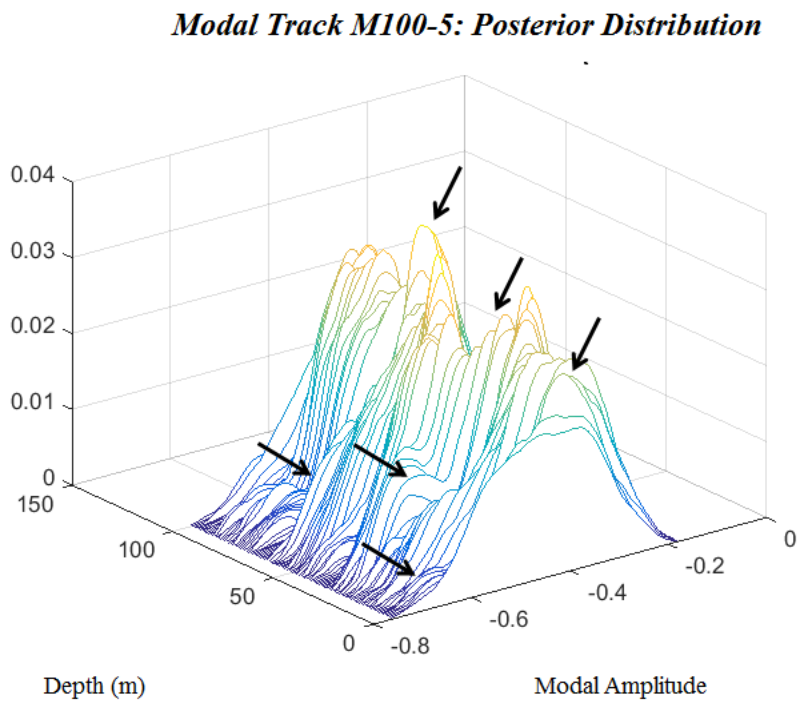

Fig. 10. Estimated multi-modal (arrows) posterior modal distribution (125-particles) surface (depth vs. amplitude vs. probability) for Mode: $M100-5$.

estimated as $(\mathrm{P_{FA}}, \mathrm{P_{DET}}) = (0.034, 0.998)$, that is, 99.8% detection with a 3.4% false alarm rate for these *SNR*s. We calculated the required thresholds of Eq. 43 for the sequential source detector and applied it to the noisy (0dB) pressure-field data shown in Fig. 4. The results for both the source present and absent scenarios are depicted in Fig. 13c,d indicating a detection in c and a non-detection (noise) in d. These results indicate the applicability of this solution to broadband source detection problem and characterize the processor performance for these *SNR*s.

V. SUMMARY

In this paper we have developed a sequential Bayesian solution to the broadband modal function tracking and pressure-field enhancement problem then coupled it to a sequential source detection scheme. Modeling a shallow ocean environment by a normal-mode propagator, we developed a broadband Bayesian solution. We showed how each of the corresponding temporal frequency bands lead to an underlying state-space structure which is used in the development of a forward propagator for signal enhancement and detection. We developed a shallow ocean simulation using SNAP, a normal-mode propagation code [31], to solve the associated boundary value problem

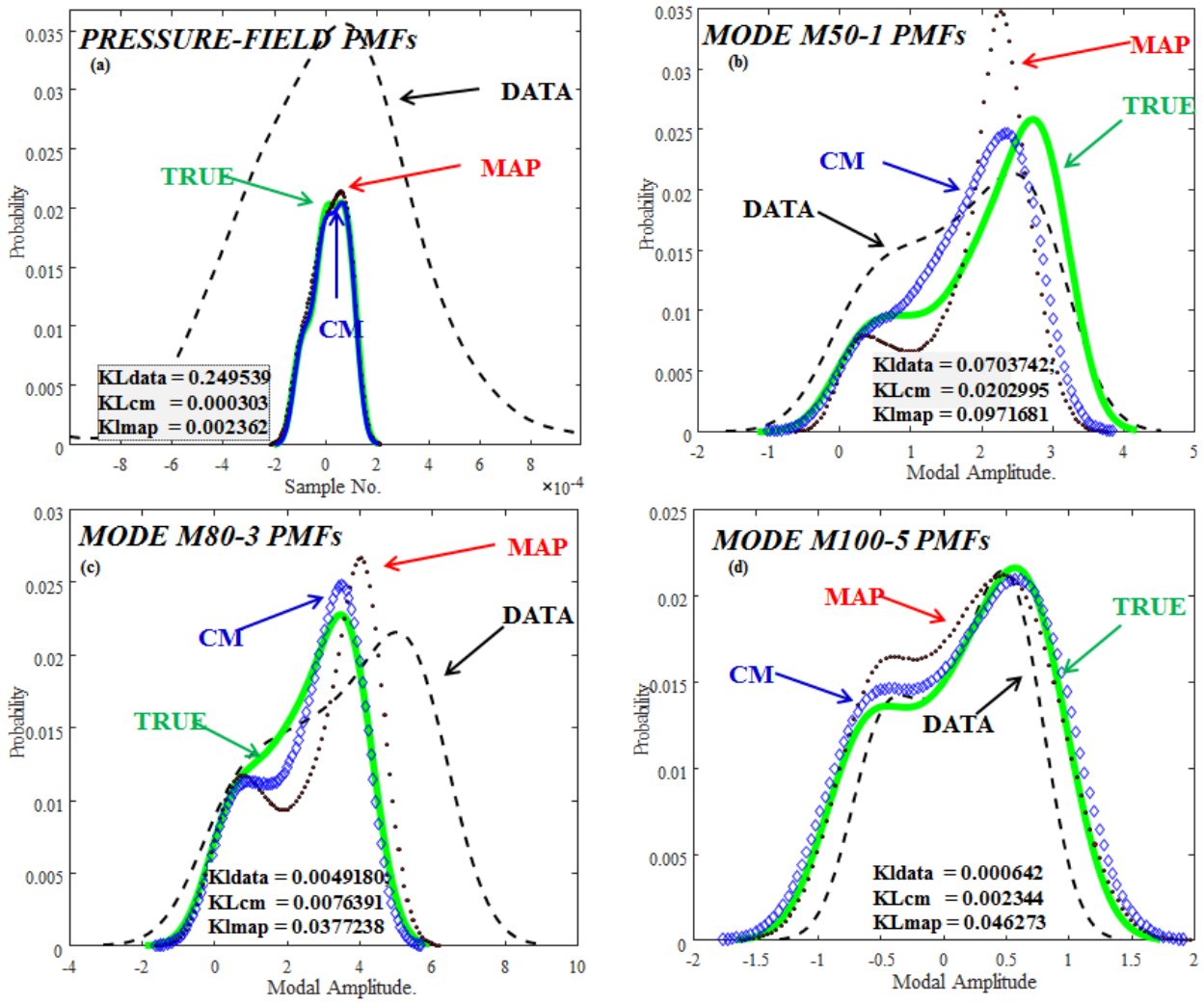

Fig. 11. Multi-modal PMF Data, True, MAP, CM estimates: (a) Pressure-field (KLcm=0.003). (b) Mode: $M50-1$ (KLcm=0.02). (c) Mode: $M80-3$ (KLcm=0.007). (d) Mode: $M100-5$ (KLcm=0.002). (125-particles).

first and supplied the resulting parameters to implement the Bayesian pre-processor. We introduced an information theoretic metric based on the Kullback-Leibler divergence statistic that can provide a reliable metric to evaluate the broadband particle filter performance for this nonstationary problem. Next we developed a sequential detector, when coupled to the pre-processor, was able to detect the broadband source in noisy pressure-field measurements and evaluated its performance from the associated *ROC* curve. We showed the results of the design demonstrating the capability of such an approach.

REFERENCES

[1] A. Parvulescu. "Signal detection in a multipath medium by MESS processing," *J. Acoust. Soc. Am.*, **29**, 223-228, 1965.

[2] C. S. Clay and H. Medwin *Acoustical Oceanography* New York: John Wiley, 1977.

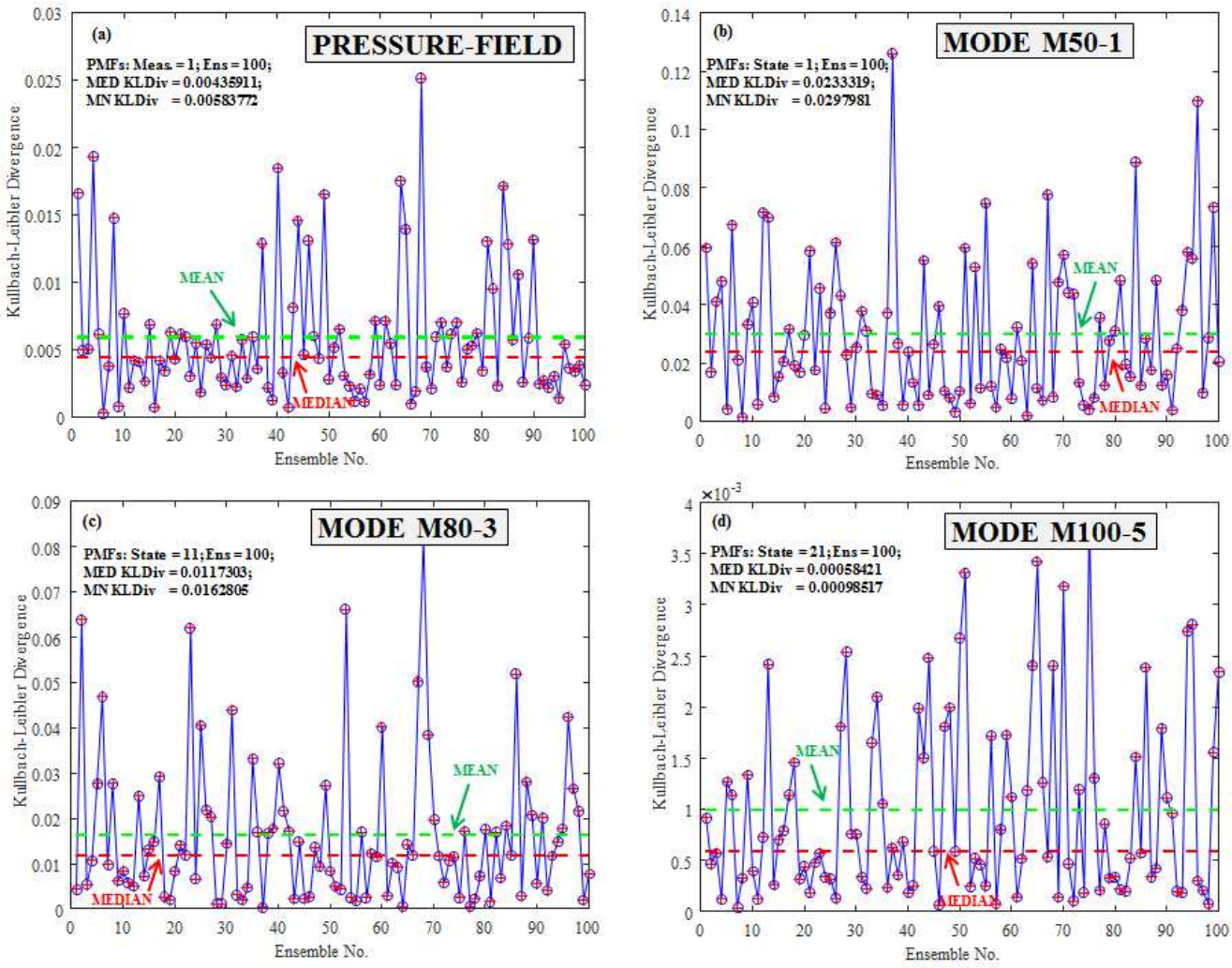

Fig. 12. Kullback-Leibler divergence trajectories (125-particles): (a) Pressure-field: True vs. MAP, CM Estimates (MED: KLDiv=0.004). (b) Mode: $M50-1$ (MED: KLDiv=0.02). (c) Mode: $M80-3$ (MED: KLDiv=0.01). (d) Mode: $M100-5$ (MED: KLDiv=0.0005).

[3] C. S. Clay. "Optimum time domain signal transmission and source localization in a waveguide," *J. Acoust. Soc. Am.*, **81**, 660-664, 1987.

[4] S. Li and C. S Clay. "Optimum time domain signal transmission and source localization in a waveguide: experiments in an ideal wedge waveguide," *J. Acoust. Soc. Am.*, **82**, 1409-1417, 1987.

[5] R. K. Brienzo and W. Hodgkiss, "Broadband matched-field processing". *J. Acoust. Soc. Am.*, **94**, 1409-1417, 1994.

[6] J. P. Hermand and W. I. Roderick, "Acoustic model-based matched-filter processing for fading time dispersive ocean channels: Theory and experiment," IEEE J. Oceanic Eng., **18**, 447-465, 1993.

[7] A. B. Baggeroer, W. A. Kuperman, and H. Schmidt, "Matched-field processing: source localization in correlated noise as an optimum parameter estimation problem," *J. Acoust. Soc. Am*, **83**, (2), 571-587, 1988.

[8] E. K. Westwood, "Broadband matched-field source localization," *J. Acoust. Soc. Am*, **91**, (5), 2777-2789, 1992.

[9] T. C. Yang. "Broadband source localization and signature estimation," *J. Acoust. Soc. Am*, **93**, (4), 1797-1806, 1993.

[10] I. T. Lu, H. Y. Chen, and P. Voltz. "A matched-mode processing technique for localizing a transient source in the time domain," *J. Acoust. Soc. Am*, **93**, (3), 1365-1373, 1993.

[11] H. Y. Chen, and I. T. Lu. "Localization of a broadband source using a matched-mode procedure in the time-frequency domain," *IEEE*

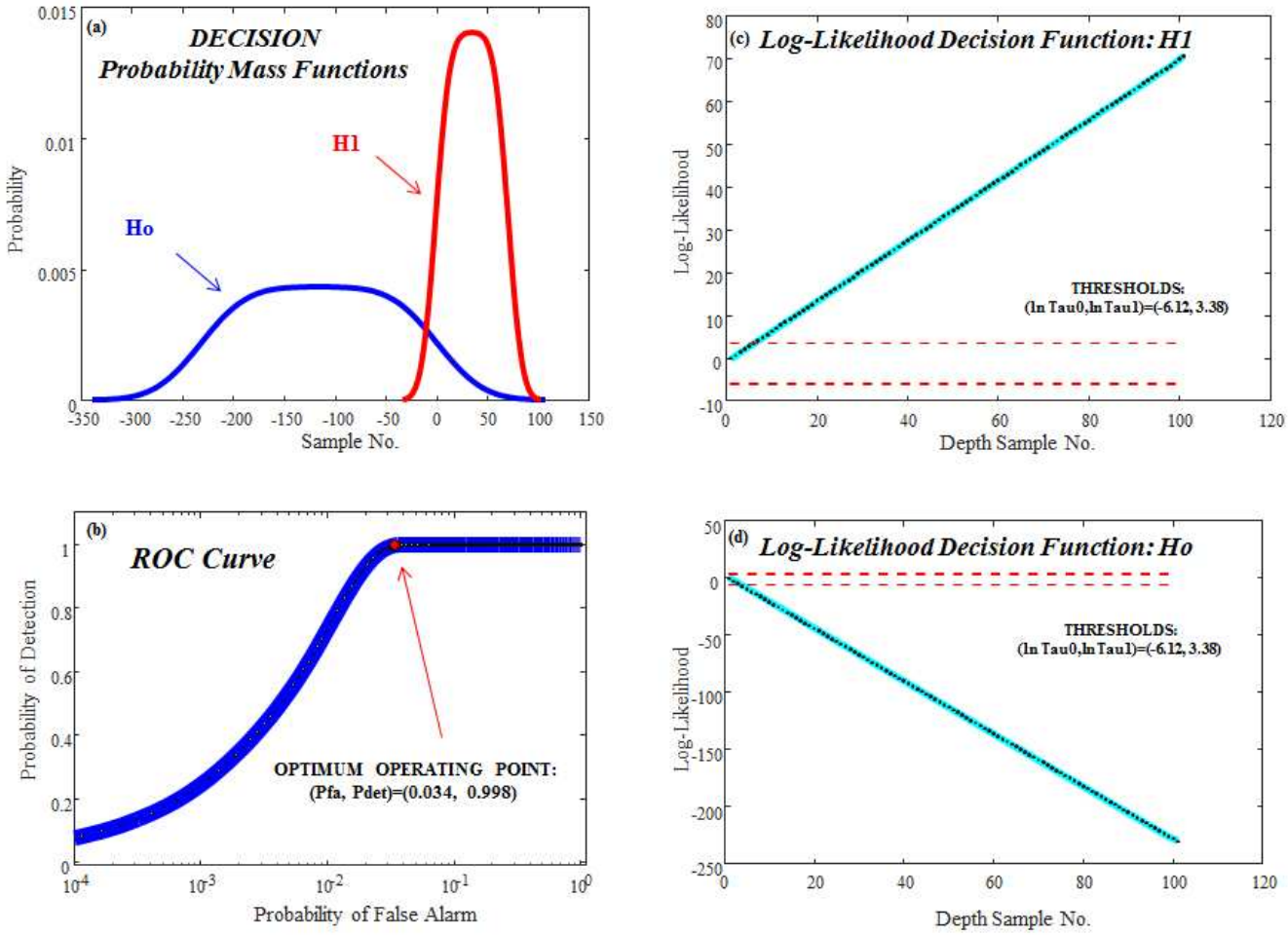

Fig. 13. Sequential detection application: (a) Log-likelihood *PMF* distributions. (b) *ROC* curve. (c) Log-likelihood decision function under hypothesis $\mathcal{H}_1$: source detection. (b) Log-likelihood decision function under hypothesis $\mathcal{H}_0$: noise.

Oceanic Engr., **19**, (2), 166-174, 1994.

[12] A. M. Richardson, and L. W. Nolte, "A posteriori probability source localization in an uncertain sound speed, deep ocean environment," *J. Acoust. Soc. Am.*, **89**, (6), 2280-2284, 1991

[13] J. V. Candy and E. J. Sullivan. "Ocean acoustic signal processing: a model-based approach." *J. Acoust. Soc. Am.*, **92**, (12), 3185-3201, 1992.

[14] J. V. Candy and E. J. Sullivan. "Broadband model-based processing for shallow ocean environments." *J. Acoust. Soc. Am.*, **104**, (1), 275-287, 1998.

[15] F. B. Jensen, W. A. Kuperman, M. B. Porter and H. Schmidt, *Computational Ocean Acoustics*. New York:AIP Press, 1994.

[16] J. V. Candy, *Model-Based Signal Processing*. Hoboken, N.J.:John Wiley/IEEE Press, 2006.

[17] W. Kuperman and F. Ingenito, "Spatial correlation of surface generated noise in a stratified ocean," *J. Acoust. Soc. Am.*, **67**, (6), 1988-1996, 1980.

[18] J. V. Candy, *Bayesian Signal Processing: Classical, Modern and Particle Filtering Methods*. Hoboken, N.J.:Wiley/IEEE Press, 2009.

[19] B. Ristic, S. Arulampalam and N. Gordon, *Beyond the Kalman Filter: Particle Filters for Tracking Applications*, Boston: Artech House, 2004.

[20] P. Djuric, J. Kotecha, J. Zhang, Y. Huang, T. Ghirmai, M. Bugallo and J. Miguez, "Particle Filtering," *IEEE Signal Proc. Mag.* vol. **20**,

No. 5, 19-38, 2003.

[21] J. V. Candy, "Environmentally adaptive processing for shallow ocean applications: A sequential Bayesian approach," *JASA*, **138**, (3), 1268-1281, 2015.

[22] J. V. Candy and E. J. Sullivan, "Passive localization in ocean acoustics: a model-based approach." *J. Acoust. Soc. Am.*, **98**, (1), 1455-1471, 1995.

[23] H. Akaike, "A New Look at the Statistical Model Identification," *IEEE Trans. Autom. Control*, Vol. 19, 1974.

[24] Y. Sakamoto, M. Ishiguro, and G. Kitagawa, *Akaike Information Criterion Statistics*, D. Reidel/Kluwer Academic, Boston, 1986.

[25] J. V. Candy, "Bootstrap particle filtering: performance of a passive synthetic aperture in an uncertain ocean application," *IEEE Signal Proc. Mag.* vol. **24**, No. 4, 73-85, 2007.

[26] H. Van Trees, *Detection, Estimation and Modulation Theory*, pt. 1, New York, New York: John Wiley, 1968.

[27] A. Wald, *Sequential Analysis*, New York, N.Y.: John Wiley, 1947 (Reprint Dover Publications, 1973).

[28] A. Papoulis and S. Pillai, *Probability, Random Variables and Stochastic Processes*, 4th ed., New York, New York: McGraw-Hill, 2002.

[29] C. Andrieu, A. Doucet, S. Singh and V. Tadic, "Particle methods for change detection,system identification and control," *Proc. IEEE*, vol. **92**, No. 3, 423-438, 2004.

[30] P. Li and V. Kadirkamanathan, "Particle methods based likelihood-ratio approach to fault diagnosis in nonlinear stochastic systems," *IEEE Trans. Syst., Man and Cyber. Pt. C*, vol. **31**, No. 3, 337-342, 2001.

[31] F. B. Jensen, and M.C. Ferla, "SNAP: the SACLANTCEN normal-mode acoustic propagation model," *SACLANTCEN Report*, **SM-121**, SACLANT Undersea Research Centre, La Spezia, Italy, 1982.

[32] M. B. Porter, "The KRAKEN normal mode program," *Report SM-245*, Italy: SACLANTCEN, 1991.

[33] H. Schmidt, "SAFARI: Seismo-acoustic fast field algorithm for range independent environments," *Report SM-245*, Italy: SACLANTCEN, 1987.

[34] E. J. Sullivan, Personal Conversation, 2016.

APPENDIX A

Central Differences for Normal-Mode State-Space

Since our array spatially samples the pressure-field discretizing depth, we choose to discretize the differential state equations of Sec. IIB using a central difference approach for improved numerical stability, we have

$$\frac{d^2\phi_m(z,\omega_q)}{dz^2} \approx \frac{\phi_m(z_\ell,\omega_q) - 2\phi_m(z_{\ell-1},\omega_q) + \phi_m(z_{\ell-2},\omega_q)}{\triangle z_\ell^2}$$

for $\triangle z_\ell := z_\ell - z_{\ell-1}$. Substituting this approximation into the modal relations gives

$$\begin{aligned} \phi_m(z_\ell,\omega_q) &- 2\phi_m(z_{\ell-1},\omega_q) + \phi_m(z_{\ell-2},\omega_q) \\ &+ \triangle z_\ell^2 \kappa_z^2(m,q)\phi_m(z_{\ell-1},\omega_q) = 0 \end{aligned}$$

where $m = 1, \cdots, M_q$ and z_ℓ is the location of the ℓ-th sensor. Defining the discrete broadband modal state vector as $\phi_m(z_\ell,\omega_q) := [\phi_m(z_{\ell-2},\omega_q) \mid \phi_m(z_{\ell-1},\omega_q)]^T$, we obtain the following set of difference equations for the m-th mode at the q-th frequency

$$\begin{aligned} \phi_{m1}(z_\ell,\omega_q) &= \phi_{m2}(z_{\ell-1},\omega_q) \\ \phi_{m2}(z_\ell,\omega_q) &= -\phi_{m1}(z_{\ell-1},\omega_q) \\ &+ \Big(2 - \triangle z_\ell^2 \kappa_z^2(m,q)\Big)\phi_{m2}(z_{\ell-1},\omega_q) \end{aligned}$$

with each of the corresponding modal A-submatrices given by

$$\mathbf{A}_m(z,\omega_q) = \begin{bmatrix} 0 & 1 \\ \\ -1 & 2 - \triangle z_\ell^2 \kappa_z^2(m,q) \end{bmatrix}; \quad m = 1, \cdots, M_q$$

APPENDIX B

Broadband Pressure-Field: State-Space Measurement Model

The pressure-field at depth z and time t can be approximated in terms of the bilateral inverse (discrete) Fourier transform (IDFT) as [34]

$$p(r,z,t) = \int_{-\infty}^{\infty} p(r,z,\omega)e^{j\omega t}d\omega \approx \frac{1}{Q}\sum_{q=-(Q-1)}^{Q-1} p(r,z,\omega_q)e^{j\omega_q t} \tag{50}$$

where the $\{\omega_q\}$ are the set of selected broadband frequencies.

Decomposing the summation into positive and negative components and using the conjugate symmetry property of the IDFT, we have

$$p(r,z,t) := p^{+}(r_s,z,t)+p^{-}(r_s,z,t)-p^{o}(r,z,t) \approx \frac{1}{Q}\Big[\sum_{q=0}^{Q-1} p(r,z,\omega_q)e^{j\omega_q t}+\sum_{q=0}^{Q-1} p^{*}(r,z,\omega_q)e^{j\omega_{-q} t}-p(r,z,\omega_0)e^{j\omega_0 t}\Big] \tag{51}$$

If we consider $p^{+}(r_s,z,t)$, then from the Helmholtz solution and the state-space model of Eq. 12 at frequency ω_q and depth z, we have that the corresponding Fourier coefficient is given by

$$p(r_s,z,\omega_q) = \mathbf{C}_{q+1}^{T}(r_s,z_s,\omega_q)\mathbf{\Phi}(z_\ell,\omega_q) \tag{52}$$

therefore, the corresponding IDFT is

$$p^{+}(r_s,z,t) = \frac{1}{Q}\sum_{q=0}^{Q-1} p(r_s,z,\omega_q)e^{j\omega_q t} = \frac{1}{Q}\sum_{q=0}^{Q-1} \mathbf{C}_{q+1}^{T}(r_s,z_s,\omega_q)\mathbf{\Phi}(z_\ell,\omega_q)e^{j\omega_q t} \tag{53}$$

Expanding this expression over q at depth z_ℓ gives

$$p(z_\ell,\Omega) := p^{+}(r_s,z_\ell,t) = \underbrace{\frac{1}{Q}\left[\mathbf{C}_1^{T}(r_s,z_s,\omega_0)e^{j\omega_0 t}\cdots\mathbf{C}_Q^{T}(r_s,z_s,\omega_{Q-1})e^{j\omega_{Q-1} t}\right]}_{\mathbf{C}(r_s,z_s,\Omega)}\underbrace{\begin{bmatrix}\mathbf{\Phi}(z_\ell,\omega_0)\\ \vdots \\ \mathbf{\Phi}(z_\ell,\omega_{Q-1})\end{bmatrix}}_{\mathbf{\Phi}(z_\ell,\Omega)} \tag{54}$$

which is the measurement model incorporated into Eq. 17.

To perform the full IDFT inversion and recover the broadband time series, then the conjugate symmetric terms of $p^{-}(r_s,z,t)$ and correction at ω_0 of $p^{o}(r,z,t)$ must also be incorporated using the state-space model.